Evaluation of Kinematics and Restraint Interaction when Repositioning a Driver from a Reclined to an Upright Position Prior to Frontal Impact using Active Human Body Model Simulations

Jonas Östh, Katarina Bohman, Lotta Jakobsson

Abstract A user expectation for future cars is being able to ride in a reclined position, which creates new challenges for how to protect the occupant in a frontal impact. Existing vehicles are designed for an upright seat position and their protection measures are likely not optimal for reclined seat positions. The present study evaluates the effect on occupant kinematics and restraint interaction using a protection strategy in which the occupant is repositioned back to an upright position prior to a frontal impact, through simulations with an Active Human Body Model. The seat-back repositioning was beneficial in that it achieved similar head kinematics during crash as in an upright initial position. Submarining of the occupant pelvis under the lap-belt was not avoided as the pelvis did not return fully to upright due to the flexibility of the lumbar spine of the HBM. The study also revealed that repositioning could be achieved by the occupant's own torso inertia during pre-crash braking as well as by moving the seat-back. Comparison of simulations with both active and passive HBM showed that the active muscles could potentially influence the crash consequence predictions from the HBM.

Keywords Occupant repositioning, reclined position, occupant kinematics, frontal impact, Active Human Body Model

I. INTRODUCTION

Future car designs include a wider scope of user expectations, such as new seating configurations and seat positions. Various concepts for Autonomous Drive (AD) vehicle interiors have shown alternative occupant compartment designs, which can allow for activities such as social interaction, with occupants riding face-to-face, working, sleeping or relaxing [1]. Several studies [1–3] have identified a user expectation to recline the seat in future cars to achieve a more relaxing and comfortable seat position. Although it is possible in many cars today to recline the front row seats extensively, few vehicles have addressed such a reclined sitting position from a crash safety perspective. Legal requirement testing and rating programs are currently only evaluating safety performance in upright seat positions.

There are several possible protection strategies related to a reclined seat-back position. A primary challenge in the reclined position is to ensure that the pelvis is restrained and to avoid submarining [4], i.e. the pelvis sliding under the lap-belt. Submarining counter-measures that rely on knee interaction to restrain the pelvis and avoid submarining might not be possible to utilize in AD vehicle seating positions [5]. In addition, the occupant torso needs to be restrained, thereby controlling occupant upper body kinematics during the impact. The present study focuses on repositioning the occupant to an upright seat position prior to the impact so that conventional strategies to protect the occupant can be utilized.

The possibility of reclined occupant positions has led to increased interest in the ability of occupant models, such as Human Body Models (HBMs) and Anthropomorphic Test Devices (ATDs), to be used for evaluation of restraint performance in reclined positions [6–7]. Authors of these initial studies reported challenges both with respect to numerical stability of Finite Element (FE) models and with the lack of validation data to validate model response. While ATDs will be necessary for verification of physical product performance, we believe that HBMs are the best available tools to be used for a reclined occupant position at present, because they are developed as general-purpose tools rather than being load-case specific. For this study an FE HBM, the SAFER HBM [8] was used, which has active muscle postural control implemented [9–10] and for which kinematics in reclined postures has recently been validated [11].

J. Östh, PhD, is a Safety Analysis CAE engineer (jonas.osth@volvocars.com, +46 728 88 91 72), K. Bohman, PhD, is a Technical Expert, and L. Jakobsson, PhD, is a Senior Technical Leader at the Volvo Cars Safety Centre, Gothenburg, Sweden. J. Östh is an Adjunct Associate Professor and L. Jakobsson an Adjunct Professor at Chalmers University of Technology, Sweden. All authors are associated with SAFER – Vehicle and Traffic Safety Centre at Chalmers in Sweden.

The study aims to answer questions on how repositioning a driver from a reclined to an upright sitting posture prior to a frontal impact would affect kinematics and restraint interaction during the crash. In addition to repositioning, combinations with other possible pre-crash interventions which can affect the occupant kinematics, such as pre-crash braking and the activation of an Electrical Reversible Restraint (ERR), were simulated. Lastly, simulations with the passive HBM was also carried out to investigate the influence of musculature on the model in these situations.

II. METHODS

Simulations were made using the explicit FE solver LS-DYNA Double Precision MPP R9.3 (LSTC, Livermore, CA, USA). A driver occupant was modelled using the SAFER HBM [8] in a car FE model, representing the driver compartment of a Volvo XC90 (Fig. 1). A vehicle fixed coordinate system with X rearward, Z upward, and Y to the right side was used (Fig. 1(a)).

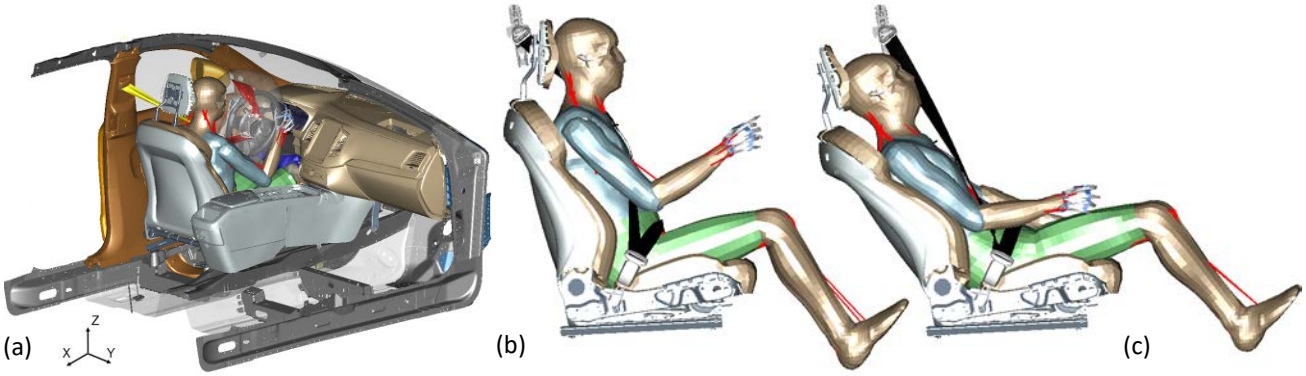

Fig. 1. (a) Volvo XC90 driver compartment FE model with the SAFER HBM positioned during the impact simulations. (b) Upright occupant position. (c) Reclined occupant position.

Occupant FE Model

The driver occupant was simulated using the SAFER HBM v9.0.1 [8,11], which is a 50th percentile HBM based on the THUMS v3 but updated by the partners of the SAFER Vehicle and Traffic Safety Centre at Chalmers in Gothenburg. In the HBM version used in the study, the head of the model has been replaced with the KTH Head Model [12] and the ribcage has been replaced with a model of a statistically based 50th percentile male shape [13]. Rib fracture prediction was done using a probabilistic method [14], using the max. first principal strain in the cortical bone for each rib [8]. In addition to these updates, the model has an updated lumbar and cervical spine compared with the THUMS v3, described in Appendix B and C of this paper. Furthermore, the SAFER HBM has an actively controlled set of lumbar, cervical, and upper extremity muscles [9–10], which models occupant reflexive responses when active or turned off for a passive model response. The reference position used for the postural controllers was the model position at the start of the simulations, i.e. the controllers try to move the HBM back to this initial posture. In the present study, when active, the upper extremity controllers were not used as the model had the hands positioned on the side of the thighs, without any support to brace against (Fig. 1(c)).

The HBM was positioned through a pre-simulation with the marionette method, applying one dimensional elements and rigid body motions to pull the HBM to the desired position. In the reclined position (Fig. 1(c)) the seat-back and torso of the HBM was reclined 20° compared with the upright reference position (27.5° seat-back angle, Fig. 1(b)), while cushion and HBM H-point positions were maintained. After the pre-simulation, stresses were not re-initialized.

Vehicle Interior FE Model

For all simulations in the present study the vehicle body in white was considered as rigid (i.e. no intrusions were considered). Vehicle crash kinematics were modelled by six-degrees-of-freedom accelerations prescribed to the vehicle rigid body. The vehicle interior surrounding the driver was modelled as deformable: the driver seat, the instrument panel, carpet, tunnel console, the door trim, and the A and B-pillar trim panels. Approximately 1.57 million elements (1.0 million shell, 0.56 million solid) were used for the interior systems and the restraints. Plastic panels were modelled using quadrilateral elements, and foam materials using tetrahedral solid elements. The vehicle interior systems, except the seat, were merged to the vehicle rigid body using the LS-

DYNA card *DEFORMABLE_TO_RIGID_AUTOMATIC during the pre-crash simulations, and switched back for the crash phase, to increase numerical stability and reduce the computational time. Although the pre-crash and crash phases are presented separately here, they were carried out in the same run without any restarting of the simulation. Active repositioning of the seat-back was made by a prescribed rotation of the recliner joint.

The restraint system modelled consisted of a driver airbag, a collapsible steering column, a knee airbag and a three-point seat-belt. For the present study, the retractor model was exchanged to a prototype FE model tuned to the same approximate performance as used in the validation, but with the ability to also simulate an Electrical Reversible Retractor (ERR) function of 180 N during the pre-crash phase. In addition, for the crash phase, a pyrotechnical pre-tensioner was modelled with the retractor. A validation of the FE vehicle and restraint system model using the Hybrid III ATD, compared with a full-scale crash test, is included in Appendix A.

Simulation Setup

For the simulations in a reclined position, three repositioning conditions were investigated: no intervention, a 20° rotation of the seat-back to the upright position over 250 ms (80°/s) or 125 ms (160/°s) at the start of the pre-crash phase. Two pre-crash scenarios were simulated. The first was without vehicle dynamics intervention, i.e. at a constant velocity. The second scenario included a maximum braking of a modern car (11 m/s^2 achieved after a 100 ms delay and then a ramp-up over 200 ms). The retractor response during the pre-crash phase was varied between a locked state and 180 N ERR activation. In addition, for ten simulations the seat-belt anchor and buckle location were varied to a position −50 mm in X and Z in the vehicle coordinate system (forward and downward) of the nominal positions. The impact simulated was a Full-Frontal Rigid Barrier impact at 56 km/h.

Table I outlines how the simulation parameters were varied. The first simulations were made with the HBM both active and passive in order to investigate the effect of the muscle activation as well as the effect of reclining the seat-back relative to an upright standard position on the crash occupant kinematics and injury prediction outcome. Later simulations were made with the active model only to also include the effect of occupant postural reflex muscle responses during the pre-crash interventions. The last eight simulations were made to investigate the effect of only the seat-back repositioning or braking on the occupant. For the simulations with the HBM active, an initial settling phase of 300 ms was simulated to initialize the muscle controllers. The settling phase was also included for the passive HBM crash simulations to provide the same initial position as the model sinks down into the seat during the settling.

TABLE I

SIMULATION MATRIX. HBM = HUMAN BODY MODEL SETTING, CV = CONSTANT VELOCITY

No.	HBM	Position	Seat-back	Retractor in Pre-Crash	Buckle and anchor	Settling (ms)	Pre-crash Motion	Pre-crash (ms)	Crash (ms)	Total Time (ms)
1	Passive	Upright	Static	No ERR	Nominal	300	None	0	120	420
2	Passive	Reclined	Static	No ERR	Nominal	300	None	0	120	420
3	Active	Upright	Static	No ERR	Nominal	300	None	0	120	420
4	Active	Reclined	Static	No ERR	Nominal	300	None	0	120	420
5	Active	Reclined	80°/s	No ERR	Nominal	300	CV	500	120	920
6	Active	Reclined	160°/s	No ERR	Nominal	300	CV	500	120	920
7	Active	Reclined	80°/s	ERR activated	Nominal	300	CV	500	120	920
8	Active	Reclined	160°/s	ERR activated	Nominal	300	CV	500	120	920
9	Active	Reclined	80°/s	No ERR	−50 mm X and Z	300	CV	500	120	920
10	Active	Reclined	160°/s	No ERR	−50 mm X and Z	300	CV	500	120	920
11	Active	Reclined	80°/s	ERR activated	−50 mm X and Z	300	CV	500	120	920
12	Active	Reclined	160°/s	ERR activated	−50 mm X and Z	300	CV	500	120	920
13	Active	Reclined	Static	No ERR	−50 mm X and Z	300	Braking	500	120	920
14	Active	Reclined	80°/s	No ERR	−50 mm X and Z	300	Braking	500	120	920
15	Active	Reclined	160°/s	No ERR	−50 mm X and Z	300	Braking	500	120	920
16	Active	Reclined	Static	ERR activated	−50 mm X and Z	300	Braking	500	120	920
17	Active	Reclined	80°/s	ERR activated	−50 mm X and Z	300	Braking	500	120	920
18	Active	Reclined	160°/s	ERR activated	−50 mm X and Z	300	Braking	500	120	920
19	Passive	Reclined	80°/s	No ERR	Nominal	0	Static	500	0	500
20	Active	Reclined	80°/s	No ERR	Nominal	300	Static	500	0	800

21	Active	Reclined	80°/s	No belt	Nominal	300	Static	500	0	800
22	Passive	Reclined	160°/s	No ERR	Nominal	0	Static	500	0	500
23	Active	Reclined	160°/s	No ERR	Nominal	300	Static	500	0	800
24	Active	Reclined	160°/s	No belt	Nominal	300	Static	500	0	800
25	Passive	Reclined	Static	No ERR	Nominal	0	Braking	500	0	500
26	Active	Reclined	Static	No ERR	Nominal	300	Braking	500	0	800
27	Active	Reclined	Static	No belt	Nominal	300	Braking	500	0	800

III. RESULTS

The pelvic angle, measured as the inclination of a vector between the mid-point of the ASIS to the pubic symphysis, relative to the vertical axis, was 52° in the upright position and 69° in the reclined position. Hence, the pelvis was reclined 17° when the HBM was positioned with the 20° reclined seat-back. In the reclined position with the nominal buckle and anchor attachment points, the buckle side of the lap-belt submarined for all simulations (Simulations 2 and 4–8), Fig. 2(b) and Table II, while this was avoided for Simulation 9–18. This means that repositioning of the seat-back to upright at 80°/s or 160°/s (Simulations 5 and 6) and in combination with ERR (Simulations 7 and 8) was not successful in preventing submarining. However, the submarining occurred later with the repositioning and more so with the faster repositioning rate.

Even though the seat-back and HBM were repositioned during the pre-crash phase for Simulations 5–8, the forced rotation of the pelvis by the repositioning was not enough to recover the upright HBM pelvic angle (Fig. 2(a)). For the 160°/s without ERR (Simulation 6) the pelvis was almost back in the upright position at 250 ms (peak rotation of −15°), but then rebounded so that it was −7° from its starting position in the reclined position when the crash phase started. Simulation 22, equivalent to Simulation 6 but with the passive HBM and only containing the pre-crash phase had a peak rotation of −12° and −5° at the end of the pre-crash phase (Fig. 2(a)). Except for this pelvic angle difference, visually there were only moderate differences in spinal curvature at the start of the crash between the repositioning Simulation 6 and the upright Simulation 3 (Fig. 3). For Simulations 7 and 8, with the ERR, the pelvis was restrained by the tensioned lap-belt and moved less toward the upright position (a final position of −4° and −7° from its starting position). For the reclined simulations (5–8) in which submarining occurred, there was more forward and downward displacement of the pelvis, than for the non-submarining, upright Simulation 3 (Fig. 2(b)).

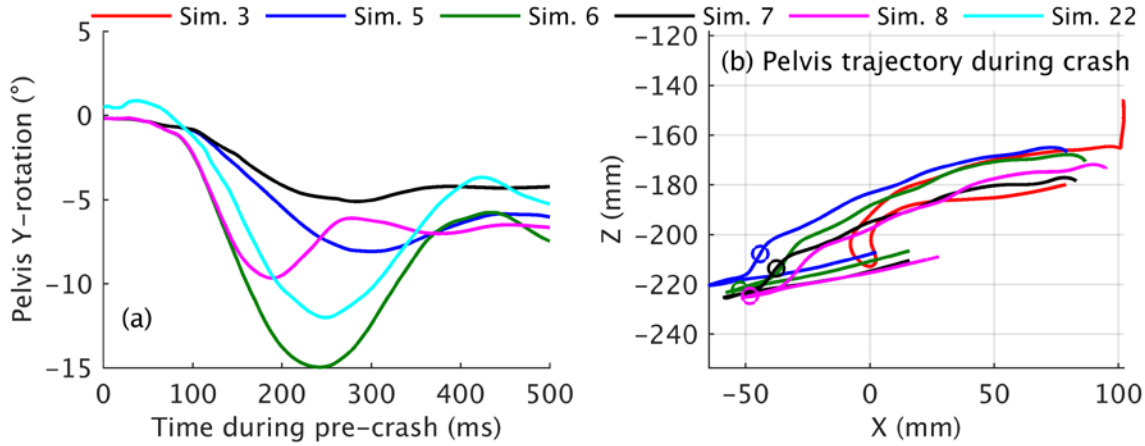

Fig. 2. (a) Dynamic pelvis rotation during repositioning in the pre-crash phase for Simulations 5–8. (b) Pelvis trajectory in the XZ-plane during the crash phase. The circles indicate the pelvis position when submarining occurred for the simulation, according to Table II.

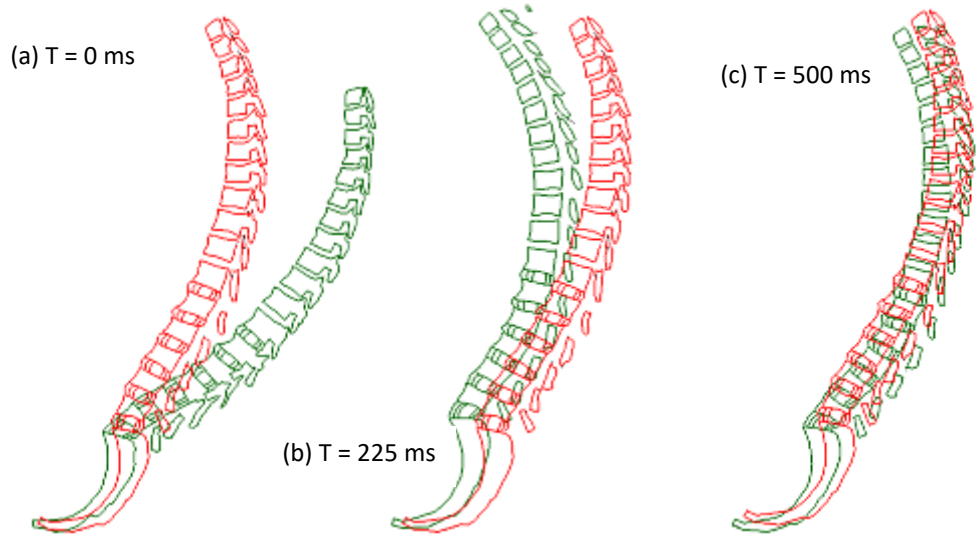

Fig. 3. T1–Sacrum spinal curvature during pre-crash phase for Simulation 6 (green) in which the seat-back is repositioned with 160°/s, compared with the spinal curvature for Simulation 3 (red) without any pre-crash maneuver. (a) Initial position, (b) max forward displacement, (c) position at end of pre-crash (start of the crash phase).

TABLE II

SUBMARINING ASSESSMENT AND INJURY PREDICTORS. CONCUSSION RISK IS FOR AIS1 CONCUSSION AND PART COLUMN INDICATE WHICH PART OF THE BRAIN THE MAX PRINCIPAL STRAIN (MPS) LEVEL ON WHICH THE PREDICTION WAS BASED WAS FOUND (GM = GRAY MATTER). NFR = NUMBER OF RIB FRACTURES. LUMBAR FZ VALUES ARE PEAK COMPRESSIVE (NEGATIVE) FORCES AND LUMBAR MY ARE PEAK FLEXION MOMENTS (POSITIVE)

	Pelvis		Head				Neck	Chest	Lumbar			
Sim.	Submarining		HIC15	Concussion	Part	MPS	Nij	NFR 2+	Fz	Level	My	Level
(-)	Buckle	Anchor	(-)	Risk (%)	(-)	(-)	(-)	45 years (%)	(kN)	(-)	(Nm)	(-)
1	No	No	298	42	GM	0.26	0.69	4	-0.99	L5	51.9	L5
2	37 ms	No	453	37	GM	0.24	0.58	85	-1.18	L5	43.9	L4
3	No	No	263	30	GM	0.22	0.55	3	-1.07	L5	54.9	L5
4	37 ms	No	478	20	GM	0.17	0.57	92	-1.12	L5	51.5	L4
5	57 ms	No	221	45	GM	0.27	0.41	14	-1.00	L5	51.5	L4
6	90 ms	No	241	25	GM	0.20	0.37	70	-1.03	L5	54.9	L4
7	57 ms	No	243	51	GM	0.29	0.44	6	-1.01	L5	53.8	L4
8	75 ms	No	264	39	GM	0.25	0.46	58	-1.09	L5	55.7	L4
9	No	No	191	42	GM	0.26	0.41	4	-1.28	L5	49.9	L5
10	No	No	234	23	GM	0.19	0.47	33	-1.42	L5	51.5	L5
11	No	No	210	49	GM	0.28	0.38	4	-1.24	L5	49.3	L5
12	No	No	223	37	GM	0.24	0.44	30	-1.27	L5	54.9	L5
13	No	No	245	29	GM	0.21	0.38	35	-1.20	L5	55.2	L4
14	No	No	207	28	GM	0.21	0.43	18	-1.24	L5	50.6	L4
15	No	No	205	27	GM	0.21	0.45	28	-1.12	L5	50.0	L4
16	No	No	302	27	GM	0.21	0.53	45	-1.64	L5	51.6	L4
17	No	No	205	44	GM	0.27	0.46	19	-1.35	L5	52.1	L5
18	No	No	216	34	GM	0.23	0.50	27	-1.28	L5	52.6	L4

A comparison of the injury predictors (Table II) between the passive HBM (Simulation 1) and the active HBM (Simulation 3) in the upright position revealed consistently lower values for the active model, except for the lumbar spine values which were slightly increased, while the in-crash kinematics were largely the same as indicated by the similar head trajectories (Fig. 4).

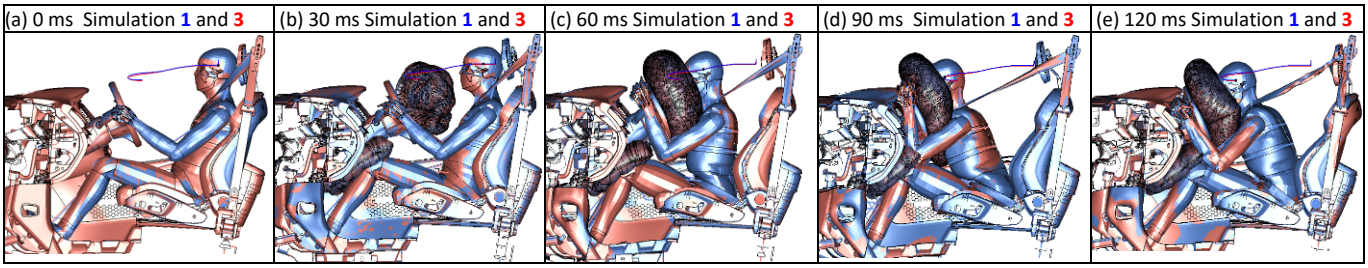

Fig. 4. Time series illustrating the upright crash kinematics of the passive HBM (Simulation 1, in blue) and the active HBM (Simulation 3, in red). The trajectory lines indicate the trajectory of the head center of gravity kinematics.

Comparing the reclined position (Simulations 2 and 4) with the upright position (Simulations 1 and 3) several injury predictors increased considerably (Table II). For instance, HIC15 increased with 155 and 215 for the passive and active model and the risk of two rib fractures or more (NFR2+) for a 45-year-old occupant increased 81% and 89%, respectively. This was due to both the submarining and increased slack in the restraint system when the occupant started further back in the crash. This can be illustrated by the difference in head X-velocity between the reclined active HBM (Simulation 4) and when the occupant was repositioned to the upright position with the changed anchor and buckle attachment geometry, which avoided submarining (Simulations 9 and 10, Fig. 5(b)). When the occupant was repositioned back to the upright position, earlier interaction with the seat-belt and driver airbag led to a lower peak head X-velocity during the crash, more like the occupant response in the upright position (Simulation 3). Also included in the Fig. is Simulation 13, which was with pre-crash braking and a locked seat-belt retractor. As can be seen from Fig. 5(a), in the repositioning simulations (Simulations 9 and 10) the HBM head had stopped moving at the end of the pre-crash phase, while due to the pre-crash braking there was about 0.8 m/s forward velocity of the HBM head in Simulation 13. All these simulations (9–18) with some sort of repositioning of the occupant to an upright position had injury prediction values more similar to the upright position (Simulation 3) than the ones in the reclined position (Simulations 2 and 4), Table II.

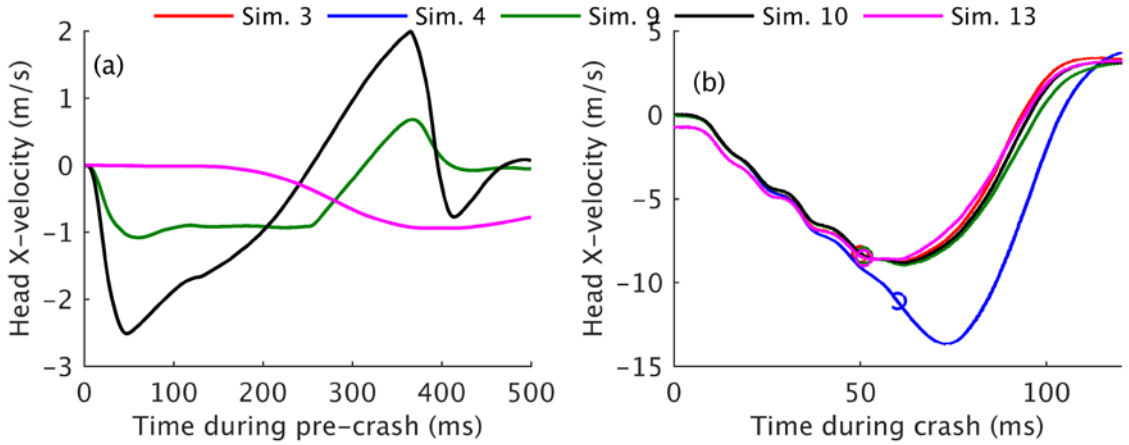

Fig. 5. (a) Head X-velocity during the pre-crash phase. (b) Head X-velocity during the crash. The circles indicate the first head contact with the inflated driver airbag.

The combination of repositioning the seatback (Simulations 9 and 10) and applying the 180N ERR (Simulations 11 and 12) lead to a similar initial crash position after 500 ms pre-crash (Fig. 6). During the repositioning phase, the head of the occupant was maximally 140 mm more forward than after 500 ms with the 160°/s (Simulation 10) seat-back repositioning (Fig. 6(b) and 7(d)). With the 180N ERR activation, this was reduced to 95 mm as the combination of tightening the belt and pushing the seatback upwards led to a shoulder belt force of 250 N at the end of the pre-crash phase in both simulations with ERR (Simulations 11 and 12).

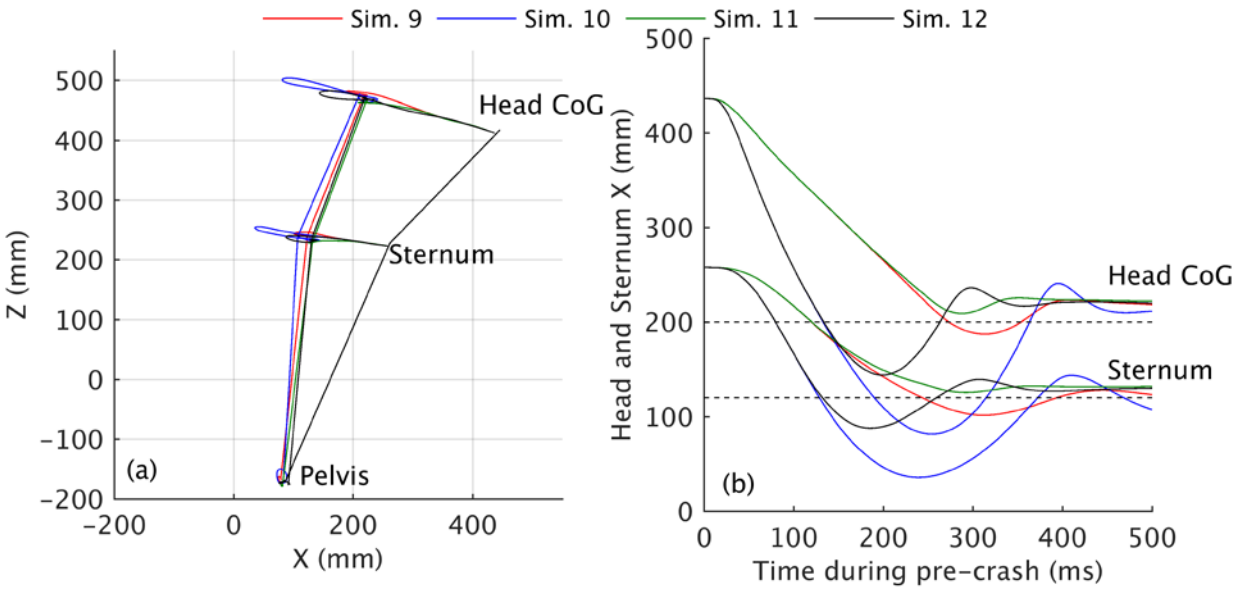

Fig. 6. (a) Head Center of Gravity (CoG), sternum, and pelvis trajectories during repositioning in the pre-crash phase for Simulations 9–12. The stick figures indicate the initial position at the beginning of the pre-crash (to the right) and at the end (to the left). (b) Head and sternum X-position during the pre-crash phase. The dashed lines show the initial head and sternum position in the upright simulations.

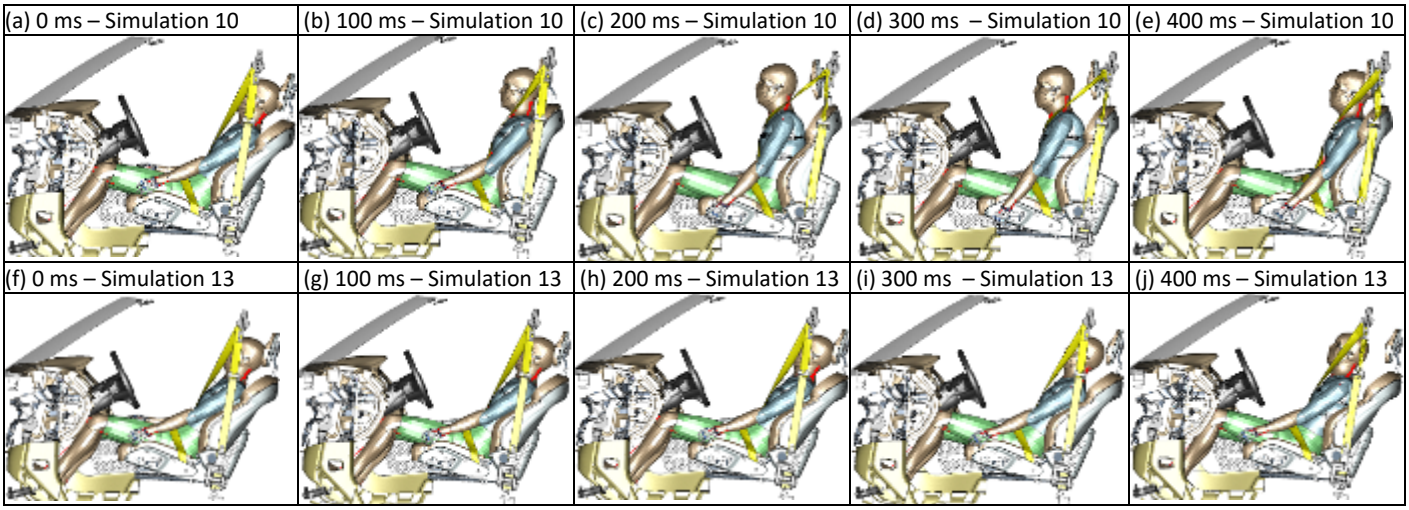

Fig. 7. Time series illustrating the pre-crash kinematics of the active HBM in: (a)–(e) Simulation 10, seat-back repositioning; (f)–(j) Simulation 13, braking.

When pre-crash braking was added in combination with repositioning, it produced the largest forward occupant displacements during pre-crash (Simulations 13–18, Fig. 8(b)). When both braking and 160°/s were applied simultaneously (Simulation 15), the head center of gravity was moved 400 mm forward from the initial reclined position and peaked 150 mm forward of the upright initial position. For all these simulations though, the HBM was rearward or at the same initial position for the head as in the upright initial position at the start of the crash (Fig. 8(b)). One exception was Simulation 14 which had not yet rebounded after repositioning at the start of the crash. Similar to the simulations without braking, Simulations 16–18 with the ERR show reduced forward overshoots as the occupant was supported by the seat-belt with a shoulder belt force of 270 N during steady state at the end of the pre-crash phase.

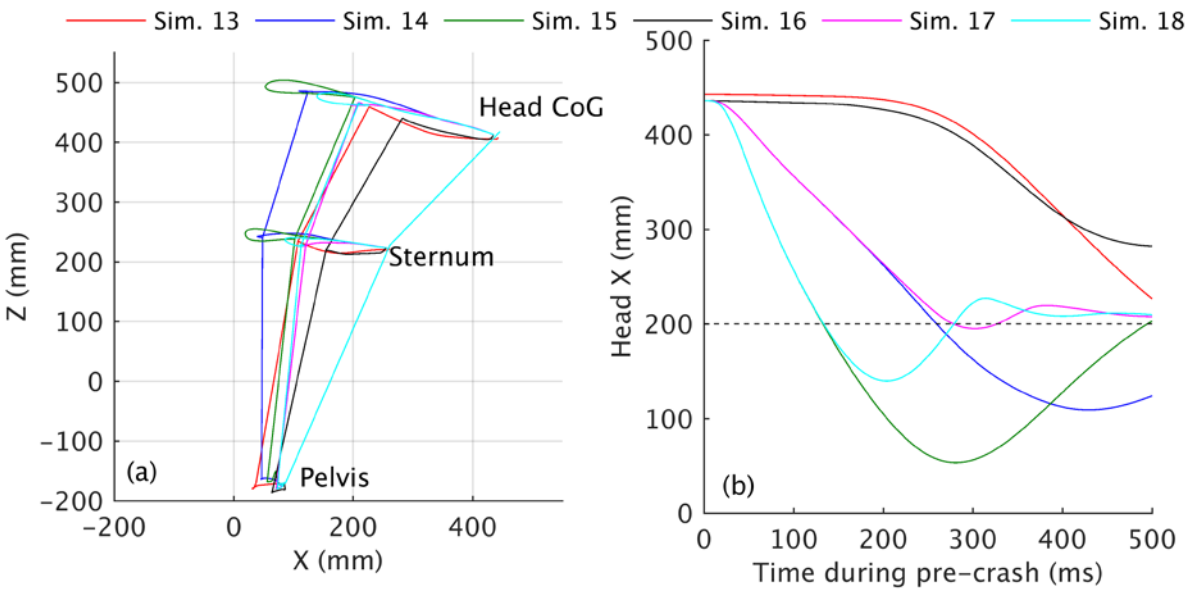

Fig. 8. (a) Head Center of Gravity (CoG), sternum, and pelvis trajectories during repositioning in the pre-crash phase for Simulations 13–18. The stick figures indicate the initial position at the beginning of the pre-crash (to the right) and at the end (to the left). (b) Head X-position during the pre-crash phase. The dashed lines show the initial head position in the upright simulations.

As indicated by the analysis of the head and sternum positions after the pre-crash phase, there was no large difference in initial position at the start of the crash phase for simulations with either a repositioning or braking intervention during pre-crash. This led to similar kinematics during the crash phase, and is visualized for Simulation 3 (upright, active HBM), Simulation 10 (repositioning at 160°/s) and Simulation 13 (pre-crash braking) in Fig. 9.

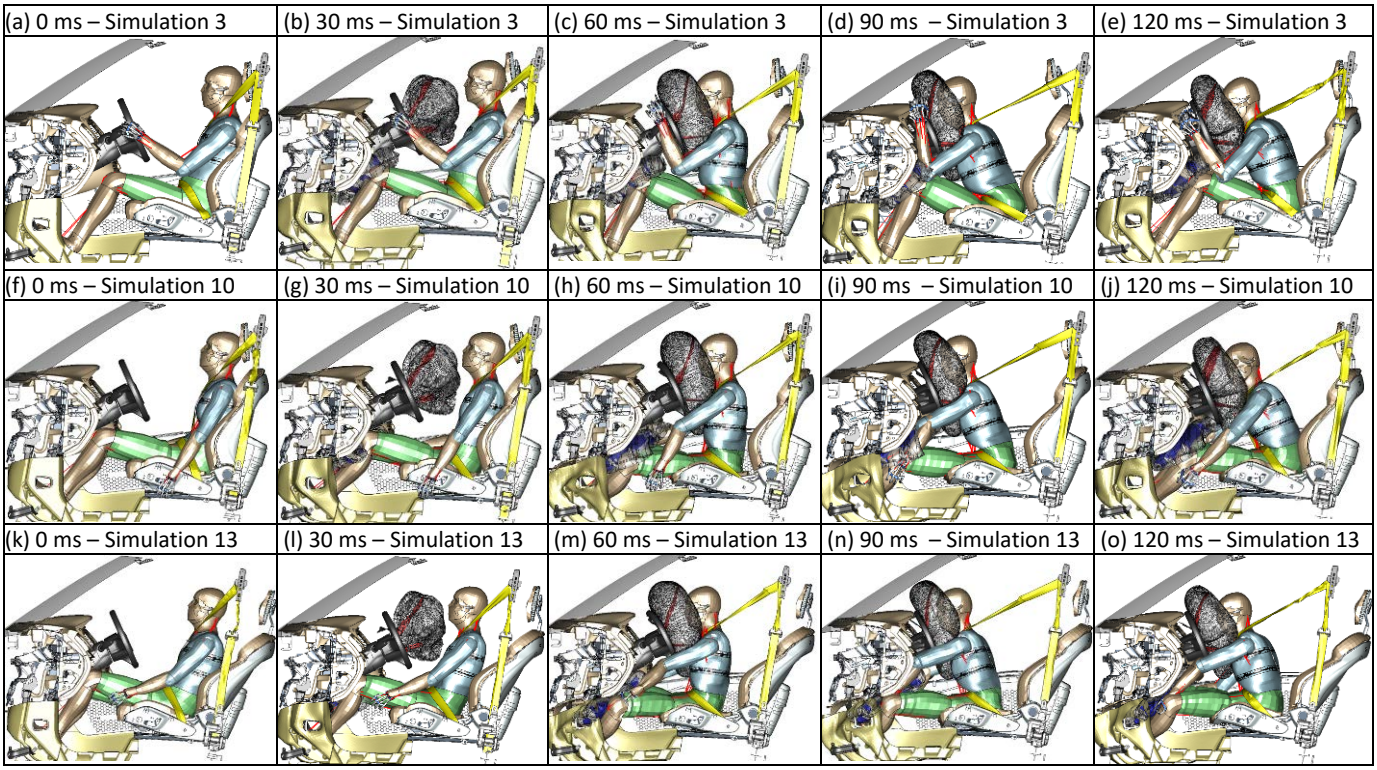

Fig. 9. Time series illustrating the crash kinematics of the active HBM in: (a)–(e) Simulation 3; (f)–(j) Simulation 10; (k)–(o) Simulation 13.

Simulations 19–24 with only the seat-back repositioning included had low injury predictor values – for example, all concussion risk predictions were below 7%, NFR 2+ rib fracture risks were 0% and lumbar loads were marginal. One exception of the predictors evaluated was Nij, which was at a maximum of 0.24 for 160°/s

with the passive HBM (Simulation 22) and 0.17 for 160°/s with active HBM (Simulation 23). Lastly, the kinematics from Simulations 21, 24, and 27, which were made without the seat-belt to show the effect of the repositioning and pre-crash braking, showed that the active HBM was able to brace and return toward the seat also without the seat-belt. This is due to the feet and legs passively reacting part of the movement, supporting the active muscle control of the upper body. For Simulation 27, braking only without the seat-belt, the occupant has not yet impacted the interior at the end of the 500 ms pre-crash simulation, but would do so after a longer simulation with the applied braking (Fig. 10(b)). Additionally, the same simulations (Simulations 19, 22, and 25) with the passive HBM are also included in Fig. 10, showing that the belted models also return to the seat during only repositioning, but that larger forward max displacements occur due to the repositioning.

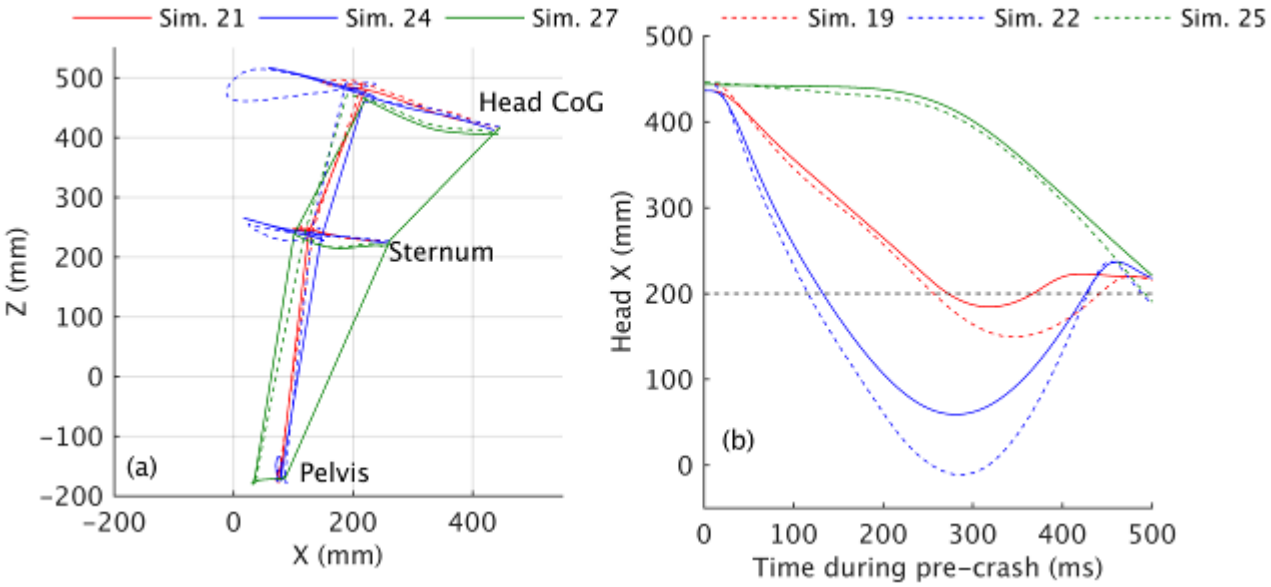

Fig. 10. Head Center of Gravity (CoG), sternum, and pelvis trajectories during repositioning in the pre-crash phase for Simulations 21, 24, and 27 with the active HBM and Simulations 19, 22, and 25 with the passive HBM. The stick figures indicate the initial position at the beginning of the pre-crash (to the right) and at the end (to the left). (b) Head X-position during the pre-crash phase. The dashed line at 200 mm show the initial head position in the upright simulations.

IV. Discussion

This study used FE simulations with a HBM in a driver compartment model to investigate the effect of repositioning an occupant from a reclined riding position to an upright position prior to a frontal crash. A HBM with active postural control [9–10] was used to enable analysis of the combined pre-crash and crash scenarios.

Repositioning the occupant prior to the crash by raising the seat-back showed that while the occupant position and spine curvature were quite similar to those in the upright position after repositioning (Fig. 2 and 3), the orientation of the pelvis was not completely restored. As a result, submarining was not avoided in the repositioning Simulations (5–8) with the nominal lap-belt anchor and buckle locations. The orientation of the pelvis relative to the lap-belt line of action has been shown to be central for the risk of submarining [15], and pushing the torso upward by the seat-back was not sufficient to reposition the pelvis as the lumbar spine of the HBM is flexible and bends into flexion. It is possible that evaluations with ATDs would have more pelvis rotation than the HBM in this respect, as they are less flexible than the HBM or PMHS (see Fig. B5 in Appendix B). As shown by the comparison between Simulation 6 (active) and Simulation 22 (passive, Fig. 2(a)), the active muscle control also contributes to how much the pelvis is repositioned (peak rotation 3° larger with active model). While the current version of the SAFER HBM could be further improved by updates to the abdominal soft tissues, its response with respect to whole body lumbar flexion was comparable to the range of PMHS responses (albeit on the stiff side, Fig. B5). The finding here that dynamic repositioning might not suffice to re-orient the pelvis could very well be valid for human occupants as well. Moreover, it was found that ERR tension of the seat-belt during the repositioning reduced the forward rotation of the pelvis somewhat. For simulations with the altered buckle and anchor geometry, the ERR activation reduced the forward displacement of the occupant during repositioning or braking.

In the present study, submarining was predicted by the HBM for the reclined positions with the nominal belt

geometry. This was partly due to the rearward rotation of the pelvis relative to the lap-belt described in the Results section but was also due to the fact that in the reclined position, the position of the lower extremities was changed so that the feet were no longer on the foot rest and pedals. As the feet were unsupported, the knees were not restrained by the knee airbag, but pushed downwards when it deployed. It is likely that the HBM would be less prone to submarining if the lower extremities were better restrained.

Repositioning the occupant by moving the seat-back in the pre-crash phase was also combined with pre-crash braking, following the logic that if the vehicle can identify a crash to reposition the seat-back, it most likely will also be able to brake to reduce the initial velocity of the crash. The results showed that the combination of both led to relatively large forward displacements of the occupant during the pre-crash phase. For the pre-crash period simulated, the HBM was able to rebound to a position like the upright position before the crash, due to restraint by the seat-belt and the muscle control in the model. It was also found that the braking alone was enough to reposition the occupant back to upright in the setup simulated here.

The different strategies of repositioning the occupant to an upright seat position resulted in reduced loading to head and chest compared to when reclined, since the restraint systems (airbag and seat-belt) used in this study are designed for an upright position. If the occupant is in the reclined position at the start of the crash, the current restraint system needs further development, to reduce the delays before they start to interact with the occupant.

In Simulations 19–27, the passive as well as the active model rebounded to the upright position after seat-back repositioning. This indicates that while the passive stiffness of the model in whole body flexion was comparable to that of PMHS (Fig. B5 in Appendix B), it might still have too large an elastic component compared with that of a passive PMHS (which would not be expected to behave in this way). Furthermore, Simulations 19–27 which were made with seat-back repositioning or braking, showed that the HBM tries to return to the seat with or without the seat-belt with the seat-back repositioning. With the pre-crash braking the active HBM was not able to do so and continued forward in the vehicle when no belt was present. The results from these seat-back repositioning only simulations show marginal injury risk predictions, which was expected as the loading level was moderate. Nevertheless, further studies are needed to investigate if there is any risk of injury due the repositioning itself; for instance, due to repeated interventions, or the potential of Whiplash Associated Disorders. Furthermore, if detailed occupant kinematics and possibly even muscle activation using normalized electromyography were recorded, such studies would be useful for further validation of active muscle control HBMs.

The active muscle control of the HBM was previously tuned and validated with respect to occupant kinematics of human volunteers subjected to maximal braking [9] in an upright position. For the present work the application range of the HBM was extrapolated to forced repositioning by moving the seat-back or braking with the occupant starting in a reclined position. The reference position used for the postural controllers was the position at the start of the simulations. Hence, the active HBM mainly tensioned the lumbar and cervical extensor muscles on the dorsal side of the body to try to get back to the reclined reference position when forced upright (Fig. D1–4 in Appendix D).

Previous impact biomechanics research with volunteers has shown that muscle activation is too slow to affect restraint forces and occupant impact kinematics in crash [16]. However, it has been indicated in FE HBM simulations that muscle activation can affect the injury outcome of a crash, for instance it can lower the external force needed to cause knee-thigh-hip fractures [17]. In the present study, the postural controllers were kept active during the crash phase of the simulations with the active HBM. A comparison of the injury predictors from Simulation 1 (passive upright) and 3 (active upright, Table II), show that the head, neck and chest predictors extracted were lower when the active muscle response was included, even though the kinematics in the simulations was not visibly different (Fig. 4). The difference between active and passive models was likely due to, first, the low-level co-contraction of 3–5% present in the model when active, which makes the muscles generate forces directly when being in eccentric contraction (forced lengthening), and, secondly, the rapid change of the control signals due to the crash dynamics. During the crash phase, the cervical extensor muscles started to react after 45 ms and the lumbar muscles after 60 ms (Fig. D5–8 in Appendix D). It should be noted, though, that when comparing the active and passive models in the reclined position (Simulations 2 and 4) the trend toward lower injury risks for the active model was not as clear, but these predictions are more spurious due to the submarining and should be treated with caution. Furthermore, the results found here that injury

predictions were lower for an active model remain to be validated with respect to human subject data, if possible, but imply the potential of HBMs that can represent live occupant responses during crash beyond most whole-body HBMs today, which are validated with respect to PMHS data. The active HBM response during the repositioning is an extrapolation of the muscle control validated for braking occupants in an upright posture. Further studies of human kinematics and muscle responses in repositioning situations are encouraged to verify or refute the response of the active HBM in this type of scenario.

V. CONCLUSIONS

In this study, the effect of repositioning a driver occupant from a reclined position to an upright position prior to a frontal impact was investigated using simulations with an active HBM. The simulations showed that in the reclined position, the model submarined under the lap-belt and a higher head impact velocity was achieved due to the greater distance to the airbag and seat-belt compared with an upright position. When the HBM was repositioned prior to crash by moving the seat-back, the higher head impact velocity was avoided due to reduced head to airbag distance. However, submarining was not avoided as the pelvis did not fully return to the upright position due to flexibility in the lumbar spine of the HBM. Adding pre-tension of the seat-belt prior to crash reduced the forward displacement of the occupant during the pre-crash phase, but also restrained the pelvis during repositioning. The study also revealed that repositioning could be achieved by the occupant's own torso inertia during pre-crash braking as well as by moving the seat-back. Comparison of simulations with both active and passive HBM showed that the active muscles could potentially influence the crash consequence predictions from the HBM.

VI. ACKNOWLEDGEMENTS

This work was done as part of the Future Occupant Safety for Crashes in Cars (OSCCAR) project, which has received funding from the European Union Horizon 2020 Research and Innovation programme under Grant Agreement No 768947. The authors would like to thank our partners at SAFER – The Vehicle and Traffic Safety Centre at Chalmers, specifically Chalmers and Autoliv Research, for their joint efforts in developing the SAFER HBM, and Svein Kleiven for the use of the KTH head model.

VII. REFERENCES

[1] Jin X, Hou H, Shen M, Wu H, Yang KH. (2018) Occupant Kinematics and Biomechanics with Rotatable Seat in Autonomous Vehicle Collision: A Preliminary Concept and Strategy. *Proceedings of the IRCOBI Conference,* Athens, Greece.

[2] Jorlöv S, Bohman K, Larsson A. (2017) Seating Positions and Activities in Highly Automated Cars – A Qualitative Study of Future Automated Driving Scenarios. *Proceedings of the IRCOBI Conference*, Antwerp, Belgium.

[3] Östling M, Larsson A. (2019) Occupant Activities and Sitting Positions in Automated Vehicles in China and Sweden. *Proceedings of the ESV Conference*, Paper no. 19-0083, Eindhoven, The Netherlands.

[4] Gepner BD, Draper D, Mroz K, Richardson R, Östling M, Pipkorn B, Forman JL, Kerrigan JR. (2019) Comparison of Human Body Models in Frontal Crashes with Reclined Seatback. *Proceedings of the IRCOBI Conference*, Florence, Italy.

[5] Rawska K, Gepner B, Kulkarni S, Chastain K, Zhu J, Richardson R, Forman J, Kerrigan JR. (2019) Submarining Sensitivity across Varied Anthropometry in an Autonomous Driving System Environment. *Traffic Injury Prevention*, **20**(Sup2): S123–127.

[6] Lin H, Gepner B, Wu T, Forman J, Panzer M. (2018) Effect of Seatback Recline on Occupant Model Response in Frontal Crashes. *Proceedings of the IRCOBI Conference*, Athens, Greece.

[7] Wang JZ, Li J, Pallavajhala K, Zhou Z, Hu J, Boyle K, Reed M. (2019) THOR 50M Suitability for Automated Vehicle Crashworthiness. *Proceedings of the ESV Conference*, Paper no. 19-0162, Eindhoven, The Netherlands.

[8] Pipkorn B, Iraeus J, Björklund M, Brunketorp O, Jakobsson L. (2019) Multi-Scale Validation of a Rib Fracture Prediction Method for Human Body Models. *Proceedings of the IRCOBI Conference,* Florence, Italy.

[9] Östh J, Brolin K, Bråse D. (2015) A Human Body Model with Active Muscles for Simulation of Pretensioned Restraints in Autonomous Braking Interventions. *Traffic Injury Prevention*, **16**(3): 304–313.

[10]Ólafsdóttir JM, Östh J, Brolin K. (2019) Modelling Reflex Recruitment of Neck Muscles in a Finite Element Human Body Model for Simulating Omnidirectional Head Kinematics. *Proceedings of the IRCOBI Conference*, Florence, Italy.

[11]Mroz K, Östling M, Richardsson R, Kerrigan J, Forman J, Pipkorn B. (2020) Effect of Seat and Seat Belt Characteristics on the Lumbar Spine and Pelvis Loading of the SAFER Human Body Model in Reclined Postures. *Proceedings of the IRCOBI Conference*, Munich, Germany.

[12]Kleiven S. (2007) Predictors for Traumatic Brain Injuries Evaluated through Accident Reconstructions. *Stapp Car Crash Journal*, **51**.

[13]Iraeus J, Pipkorn B. (2019) Development and Validation of a Generic Finite Element Ribcage for Strain Based Fracture Prediction. *Proceedings of the IRCOBI Conference,* Florence, Italy.

[14]Forman JL, Kent RW, Mroz K, Pipkorn B, Bostrom O, Segui-Gomez M. (2012) Predicting Rib Fracture Risk with Whole-Body Finite Element Models: Development and Preliminary Evaluation of a Probabilistic Analytical Frame Work. *Annals of Advances in Automotive Medicine*, **56**:109–124.

[15]Uriot J, Baudrit P, Potier P, Trosseille X, Petit P, Guillemot H, Guerin L, Vallancien G. (20069 Investigations on the Belt-to-Pelvis Interaction in the Case of Submarining. *Stapp Car Crash Journal* **50**:53–73.

[16]Begeman PC, King AI, Levine RS, Viano DC. (1980) Biodynamic Response of the Musculoskeletal System to Impact Acceleration. *Proceedings of the 24th Stapp Car Crash Conference*, Troy, MI, USA.

[17]Chang CY, Rupp JD, Kikuchi N, Schneider LW. (2008) Development of a Finite Element Model to Study the Effects of Muscle Forces on Knee-Thigh-Hip Injuries in Frontal Crashes. *Stapp Car Crash Journal* **52**:475–504.

VIII. Appendix A – Restraint and Interior FE Model Validation

The vehicle interior and restraint FE model were validated using a simulation with the Hybrid III ATD (v7.1.2, Humanetics ATD, Heidelberg, Germany), compared with a full-scale crash test run at Volvo Cars Safety Centre (VCSC). The load case simulated for the validation was a 64 km/h Offset Deformable Barrier impact. The correlation between test and simulation (Fig. A1), was high for most responses, indicating that the FE model used for the present study was a good representation of a real vehicle's interior and restraint system during impact.

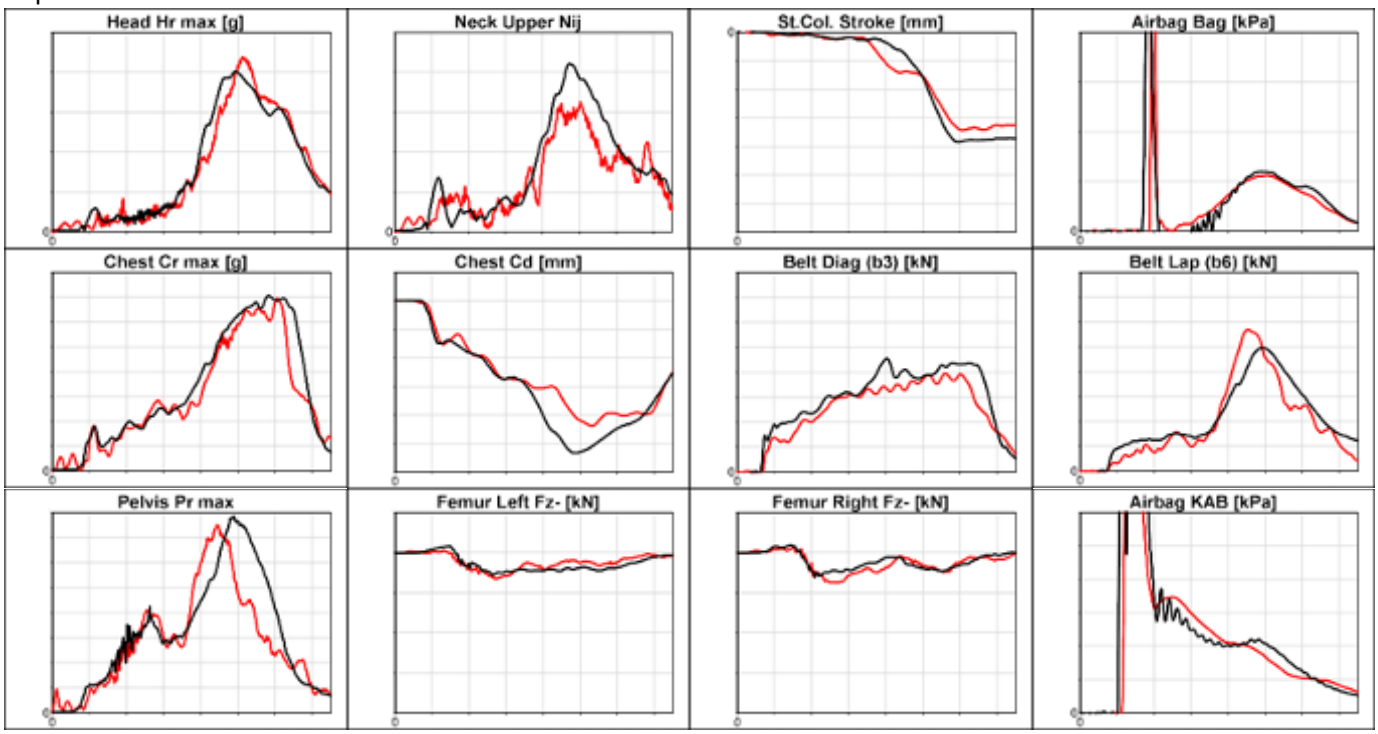

Fig. A1: Vehicle interior FE model with a Hybrid III ATD in a simulation (red) compared with a full-scale crash test run at the VCSC (black). Axes blanked out so as not to disclose the performance of the vehicle.

IX. Appendix B – Lumbar Spine Update

The original lumbar spine in the HBM (Fig. B1(a)) had rigid vertebrae. For the present study, the surface quadrilateral shells were changed to a linear elastic cortical bone material (E=17.1 GPa, ν=0.3 [18]) with a uniform thickness of 1 mm, while the vertebral endplates were kept rigid. In addition, the contact thickness of the cortical bone was increased to 2 mm to reduce the distance between the vertebrae. The hexahedral elements in the vertebrae was assigned E=0.283–0.328 GPa and ν=0.3 based on trabecular bone stiffness [19] as a function of bone mineral densities reported by Yoganandan *et al.* [20].

New composite intervertebral discs [21–22] were created from sacrum to the T12 vertebra, filling the space between the vertebral endplates (Fig. B1). The discs were modelled with two rings of annulus fibrosus ground substance and a viscoelastic nucleus pulposus center with material parameters from [23]. Three double layers of annulus fibrosus fibers were modelled with a non-linear orthotropic material model [23], with stress-strain data from Holzapfel *et al.* [24] and fiber directions from Cassidy *et al.* [25]. The intervertebral discs were constrained to move with the rigid endplates.

The intervertebral ligaments of the lumbar spine: the Anterior Longitudinal Ligament, Posterior Longitudinal Ligament, Capsular Ligament, Ligamentum Flavum, Supraspinal Ligament, Interspinous Ligament, and the Intertransverse Ligament, were remodeled using one-dimensional beam elements with adjusted origin and insertion points so that the ligaments had similar lengths as reported by Pintar *et al.* [26]. Non-linear stress-strain data for the ligaments were based on linear stiffnesses [26], with an assumed toe region up to 2% strain with 10% of the linear stiffness. At 90% of the reported failure strain [26], the stiffness was assumed to decrease to 10% of the linear stiffness until the failure strain. Data for the Intertransverse Ligament were not reported by [26], therefore it was assumed to have the same tensile characteristics as the Posterior Longitudinal Ligament and a cross-sectional area of 6 mm^2 [27]. When several beam elements were used to represent one ligament, the cross-sectional area [26] was divided equally between the elements.

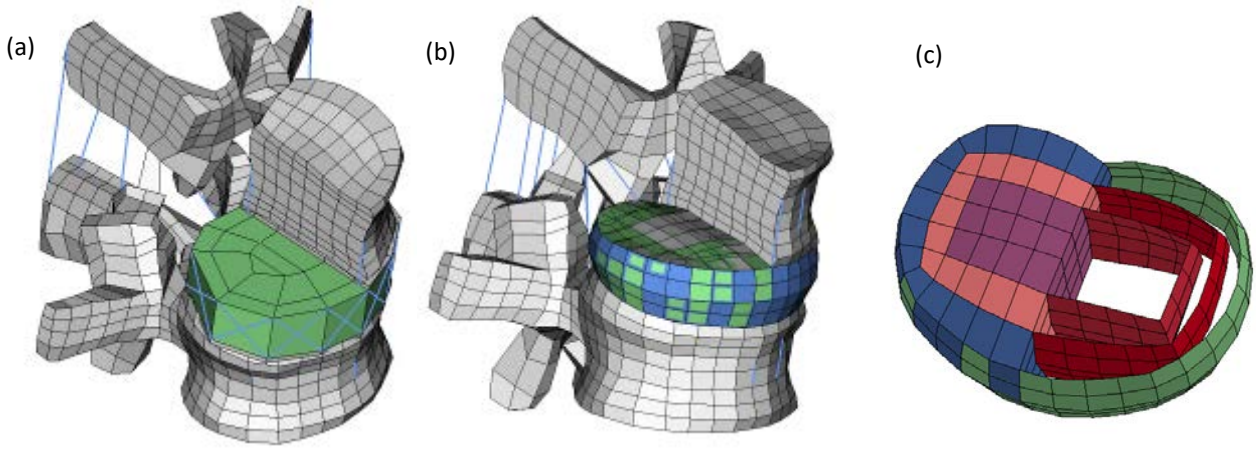

Fig. B1. (a) The original L2–L3 Functional Spine Unit (FSU), (b) updated L2–L3 FSU developed and used for the present study, and (c) the new intervertebral disc structure.

The mechanical properties of the updated lumbar spine were assessed for the L2–L3 Functional Spine Unit (FSU): Intervertebral rotations were compared with respect to quasi-static step-wise applied loading test data from [28] (Fig. B2) and compression and tension cyclic loading tests [29] (Fig. B3). In flexion and extension, the non-linear characteristics of the FSU were similar to the corridors from the test data [28] (Fig. B2(a)) but the response curve was shifted 2° below the experimental curve, indicating that what was considered as the neutral position was different between simulation and test. In compression and tension cycling (Fig. B3) the FSU had a similar stiffness as the test data for approximately −1.5–0.5 kN load, while outside this range it was somewhat too stiff.

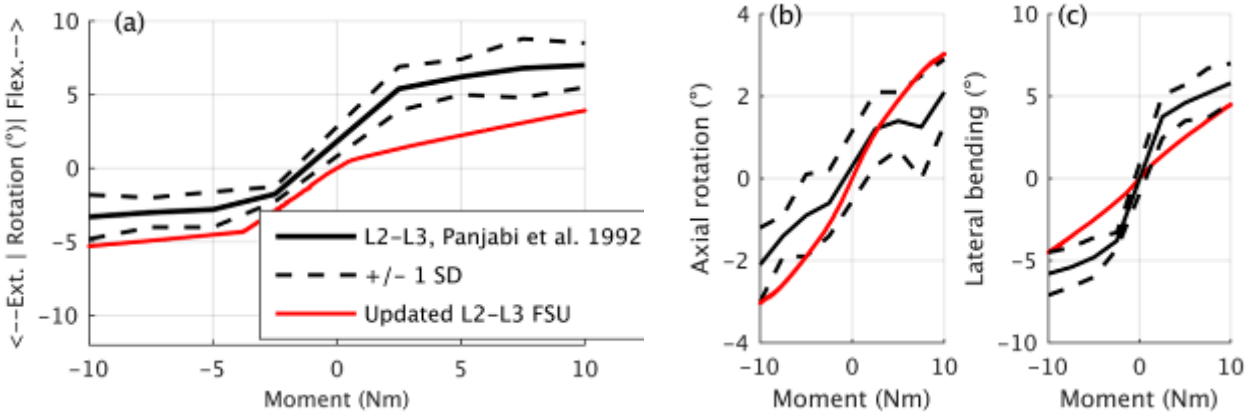

Fig. B2. (a) L2–L3 Functional Spine Unit (FSU) response to stepwise applied Flexion (Flex.) and Extension (Ext.) moments compared with experimental data from Panjabi *et al.* [28]. L2–L3 FSU response to stepwise axial rotation (b) and lateral bending moments (c) compared with test data from [28]. SD = Standard Deviation.

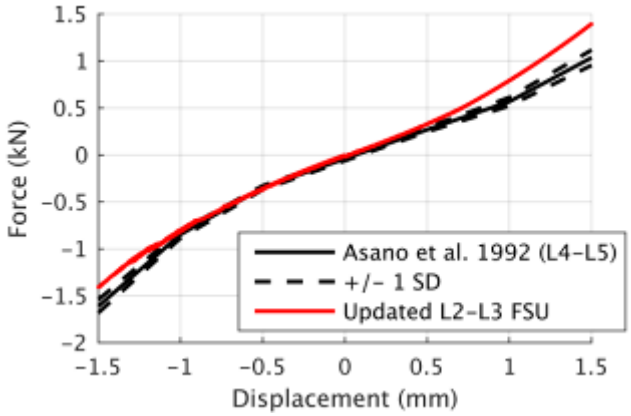

Fig. B3. Compression and tension cyclic loading with the updated L2-L3 FSU in comparison with experimental data from Asano *et al.* [23]. SD = Standard Deviation.

The response of the assembled L5–T12 ligamentous lumbar spine was assessed with respect to corridors from dynamic tests performed by Demetrepoulos *et al.* [30]. A displacement of 100 mm/s was applied to the L5 vertebra of the model, while the T12 vertebra was fixed, similar to the experimental boundary conditions. The results from the simulations (Fig. B4) revealed that most degrees of freedom (DOF) tests evaluated had non-linear characteristics similar to and within the test corridors, but that the updated lumbar spine was too compliant in extension and lateral bending. A likely explanation for this was that the facet joint cartilages were not included in the model, which left excessive play between the vertebrae in extension and lateral bending rotation motions.

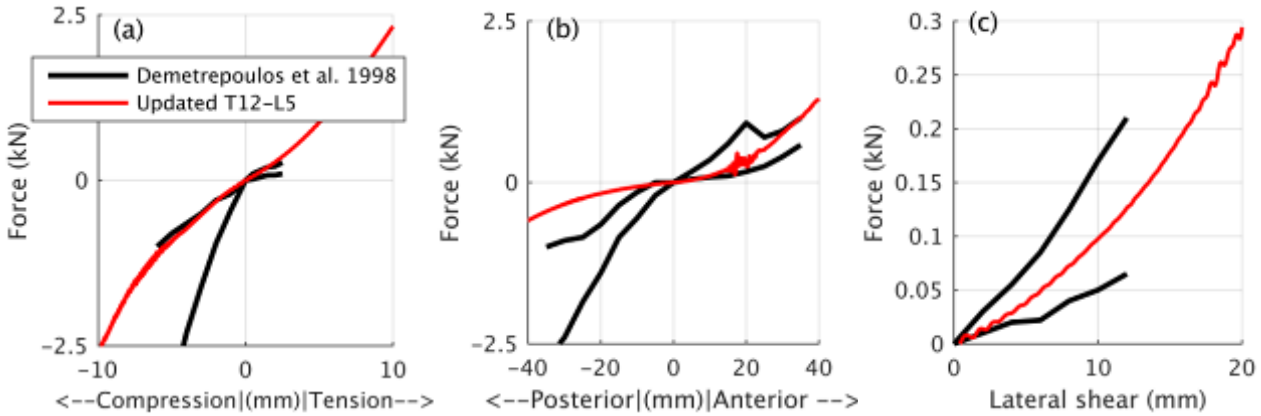

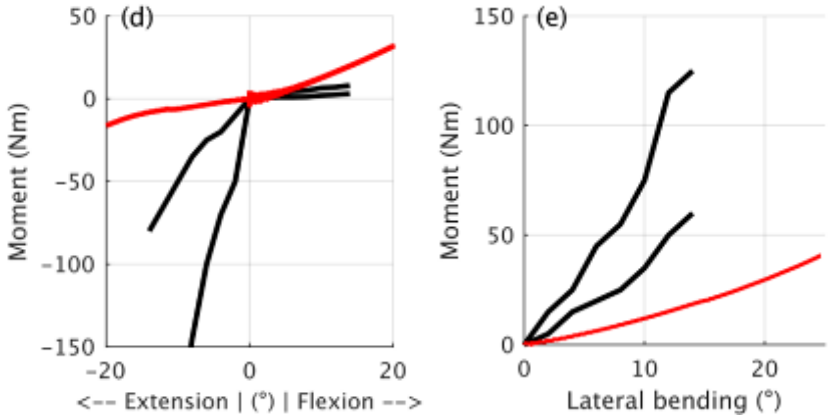

Fig. B4. The assembled L5–T12 ligamentous lumbar spine in comparison with response corridors from PMHS spines tested by Demetrepoulos *et al.* [30]. (a) Compression-tension. (b) Anterior-posterior shear. (c) Lateral shear. (d) Flexion-extension rotation. (e) Lateral bending.

Lastly, the response of the whole HBM with the updated lumbar spine was evaluated for quasi-static lumbar flexion. The simulation setup was a simplified version of the experimental one used by Uriot *et al.* [31] for the Hybrid II, Hybrid III, and THOR dummies and nine PMHS. The femora of the HBM were constrained and a rigid body with a rotation center located in space at the sacral endplate was used to force the upper body (by a joint at the T7 vertebra) into lumbar flexion at 14°/s for a 2 s simulation duration. The whole HBM with the updated lumbar spine was more compliant than the dummies evaluated by Uriot *et al.* [31] and was close to the upper corridor limit of the PMHS responses (Fig. B5.) The kink in the curve up until 4° flexion was due to dynamic effects while accelerating the trunk of the model. Simulations at faster rates (28°/s and 56°/s, results not shown) had significantly larger dynamic effects, and the 14°/s was considered close enough to be compared with the quasi-static test data.

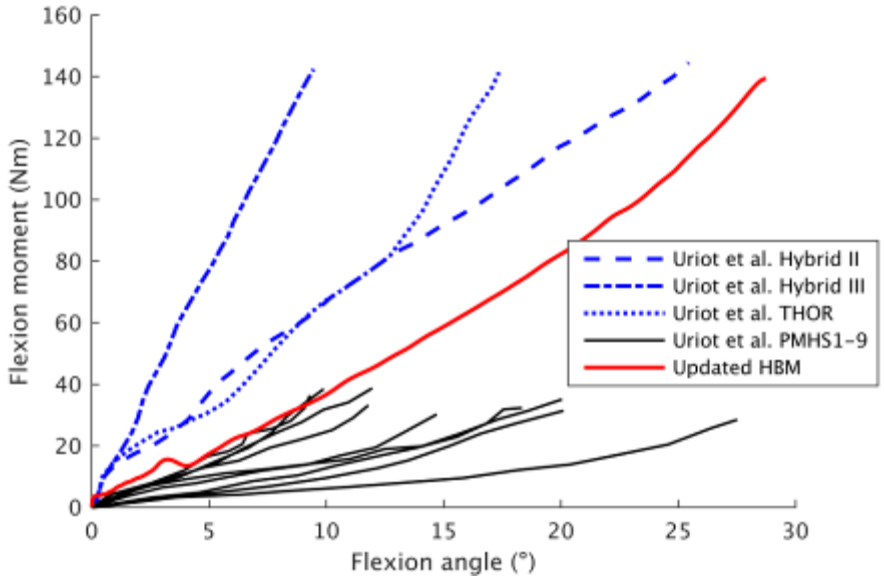

Fig. B5. The complete human body model subject to forced lumbar flexion in quasi-static conditions, similar to the setup used by Uriot *et al.* [31].

Appendix B References

[18]Reilly DT, Burstein AH, Frankel VH. (1974) The Elastic Modulus for Bone. *Journal of Biomechanics*, **7**(3):271–275.

[19]Kopperdahl DL, Keaveny TM. Yield Strain Behavior of Trabecular Bone. (1998) *Journal of Biomechanics,* **31**(7):601–608.

[20]Yoganandan N, Pintar FA, Stemper BD, Baisden JL, Aktay R, Shender BS, Paskoff G, Laud P. (2006) Trabecular Bone Density of Male Human Cervical and Lumbar Vertebrae. *Bone*, **39**(2):336–344.

[21]Halldin PH, Brolin K, Kleiven S, von Holst H, Jakobsson L, Palmertz C. (2004) Investigations of Conditions that Affect Neck Compression Flexion Injuries using Numerical Techniques. *Stapp Car Crash Journal*, **44**:127–138.

[22]Panzer MB and Cronin DS. (2009) C4–C5 Segment Finite Element Model Development, Validation, and Load-Sharing Investigation. *Journal of Biomechanics*, **42**:480–490.

[23]Östh J, Brolin K, Svensson MY, Linder A. (2016) A Female Ligamentous Cervical Spine Finite Element Model Validated for Physiological Loads. *Journal of Biomechanical Engineering*, **138**.

[24]Holzapfel GA, Shulze-Bauer CAJ, Feigl G, Regitnig P. (2005) Single Lamellar Mechanics of the Human Lumbar Anulus Fibrosus. *Biomechanical Modeling in Mechanobiology*, **3**(3):125–140.

[25]Cassidy JJ, Hiltner A, Baer E. Hierarchical Structure of the Intervertebral Disc. (1989) *Connective Tissue Research*, **23**(1):75–88.

[26]Pintar FA, Yoganandan N, Myers T, Elhagediab A, Sances A. (1992) Biomechanical Properties of Human Lumbar Spine Ligaments. *Journal of Biomechanics*, **25**:1351–1356.

[27]Eberlein R, Holzapfel GA, Fröhlich M. (2004) Multi-segment FEA of the Human Lumbar Spine Including the Heterogenity of the Annulus Fibrosus. *Computational Mechanics*, **34**:147–163.

[28]Panjabi MM, Oxland TR, Yamato I, Crisco JJ. (1994) Mechanical Behavior of the Human Lumbar and Lumbosacral Spine as Shown by Three-Dimensional Load-Displacement Curves. *Journal of Bone and Joint Surgery (Am)*, **76**:413–424.

[29]Asano S, Kaneda K, Umehara S, Tadano S. (1992) The Mechanical Properties of the Human L4-L5 Functional Spinal Unit During Cyclic Loading – The Structural Effects of the Posterior Elements. *Spine*, **17**(11):1343–1352.

[30]Demetrepolous CK, Yang KH, Grimm MJ, Khalil TB, King AI. (1998) Mechanical Properties of the Cadaveric and Hybrid III Lumbar Spine. *Stapp Car Crash Journal*, **42**.

[31]Uriot J, Potier P, Baudrit P, Trosseille X, Richard O, Douard R. (2015) Comparison of HII, HIII and THOR dummy responses with respect to PMHS sled tests. *Proceedings of the IRCOBI Conference,* Lyon, France.

X. Appendix C – Cervical Spine Update

The cervical spine, from the C7–T1 intervertebral disc to the occipital condyles (C0) was updated in a similar manner as the lumbar spine described in Section IX, Appendix B. The vertebrae were changed from rigid to linear elastic and a uniform cortical thickness of 1 mm, while the end plates were kept rigid. Similar to the lumbar spine, the contact thickness was increased to 2 mm. Trabecular bone stiffness was based on bone mineral density values for male cervical spines [32], resulting in E=0.327–0.495 GPa [19] from C1 to C7. Different from the lumbar spine, the original HBM lower cervical spine had solid cartilage blocks representing the facet joints. These were converted to sliding contact joints by splitting and separating the elements by 1 mm half way through the elements (Fig. C1(a) and (c)). The facet cartilages were changed from linear elastic to a Fu-Chang foam material with an approximate initial stiffness of 10 MPa up to 10% strain, but with much higher stiffness at larger strains (A1=0.001 GPa, A2=0.0011 GPa and B1=B2=7) and selective reduced integration (ELFORM=2) to avoid numerical issues during large compressive forces on the facets. The intervertebral discs were modelled using the same method and material data as described in Section IX above.

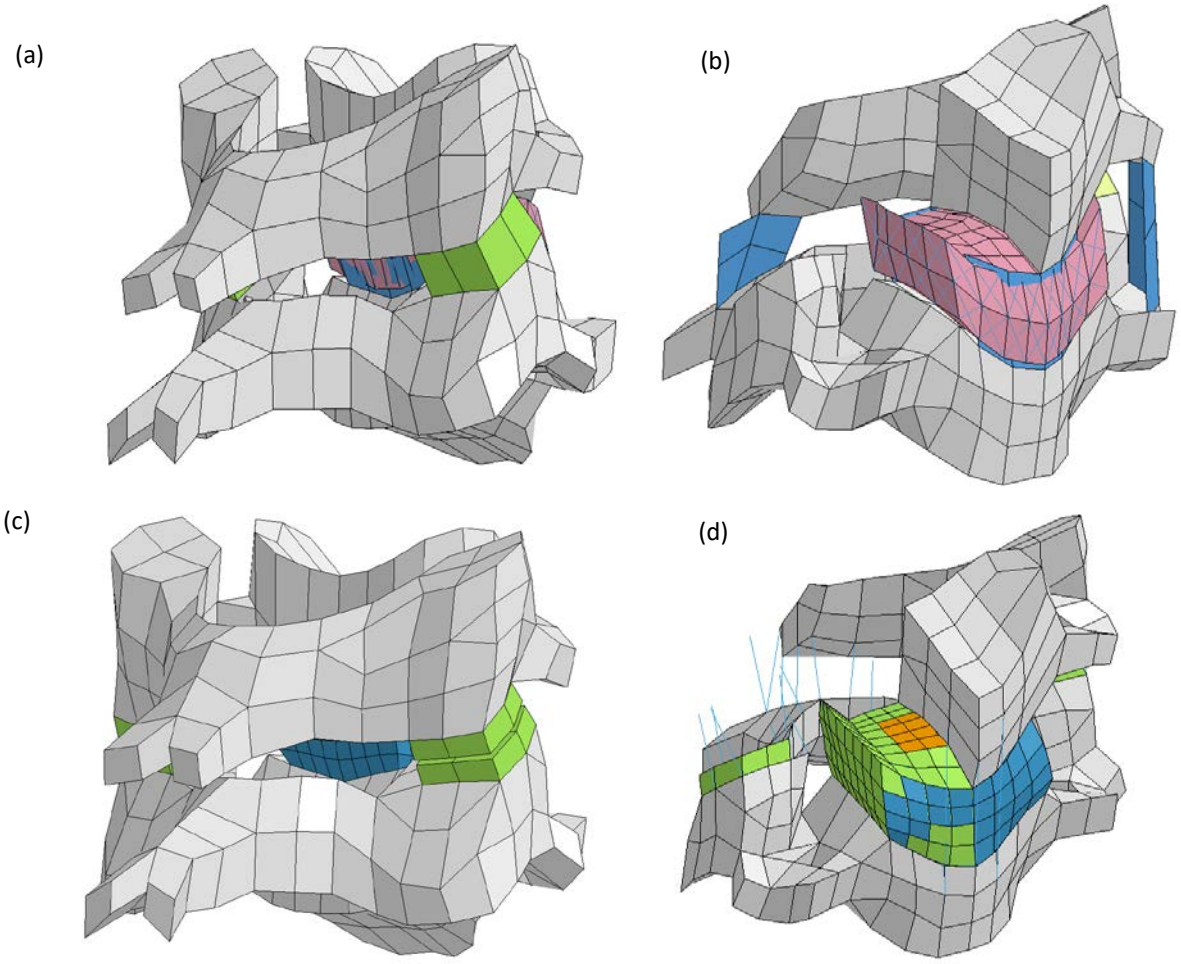

Fig. C1. (a)–(b) Original C4–C5 Functional Spine Unit (FSU). (c)–(d) Updated C4–C5 FSU used for the present study.

The shell meshed linear elastic ligaments of the original model (Fig. C1(b)) were replaced by one dimensional non-linear beam elements (Fig. C1(d)). Cross-sectional areas and lengths of the ligaments were based on data from [33]. Non-linear tensile properties for the lower cervical spine was based on [34] and for the upper cervical spine on [35] and [36].

The responses of a selected updated FSU, at the C4–C5 level, and the upper cervical spine, C0–C2, were assessed with respect to experimental data from [37] and [38] for the rotational DOF (Fig. C2). For the C4–C5 FSU the rotational DOFs showed the same non-linear shape as the experimental data around the neutral position. The C0–C2 upper cervical spine had a too low range of motion in flexion, and the axial rotation response was somewhat too stiff close to the neutral position, but seemed to be approaching the axial rotation

range of motion indicated by the experimental curve at moments larger than 3 Nm. For the upper cervical spine, C0–C2, all three signals were noisy due the contact between the vertebrae which consist of a coarse stiff mesh (no articular cartilages were included in the model at this vertebral level). Furthermore, the C4–C5 FSU translational DOFs compliances were evaluated at 25 N loading, and compared with data from [39] (Fig. C3). The C4–C5 FSU model was too stiff in tension, while in compression it was close to the average experimental response. In posterior shear the model was too compliant, while the other shearing DOFs were within the experimental variation.

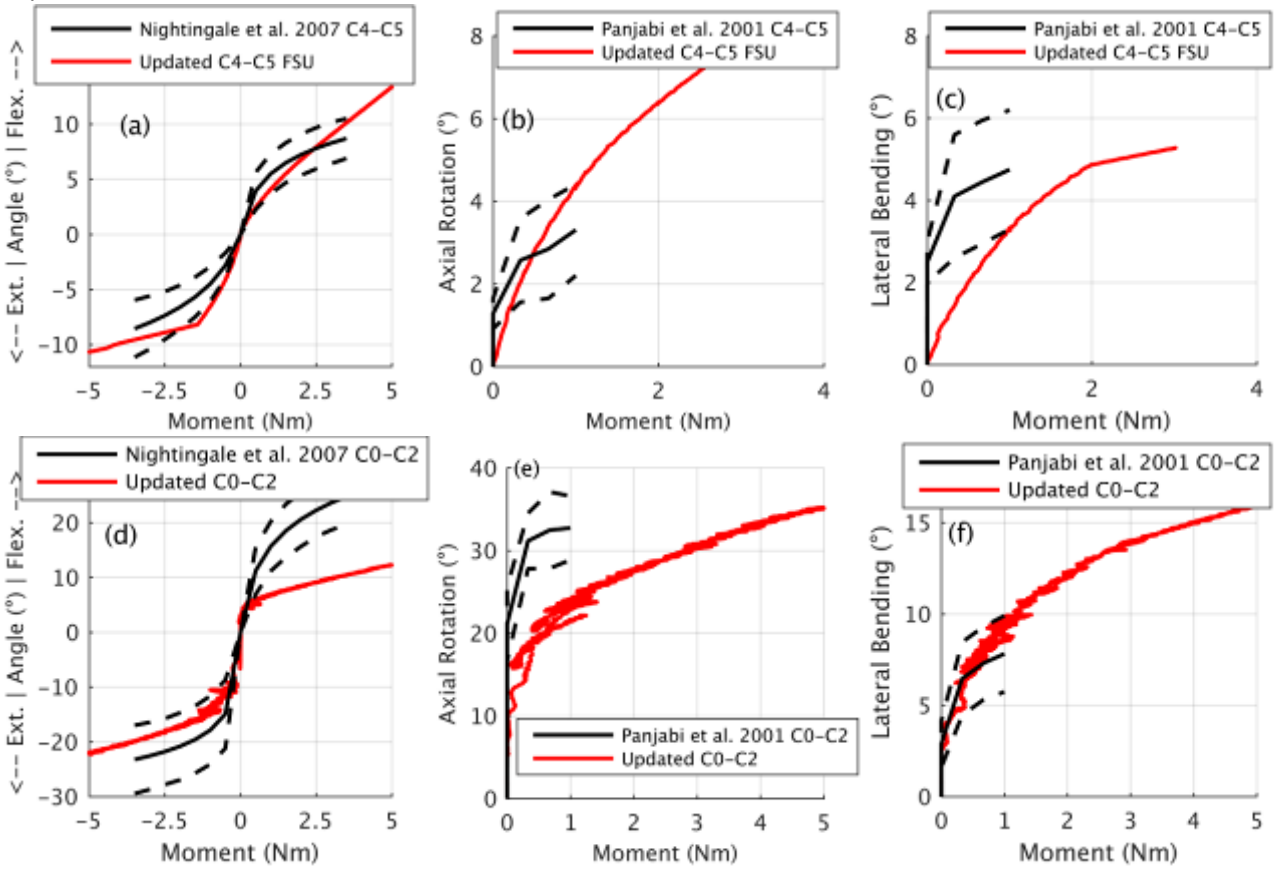

Fig. C2. The updated C4–C5 FSU in (a) Flexion (Flex.) and Extension (Ext). rotational loading in comparison with experimental data from Nightingale *et al.* [38], (b) axial rotation and (c) lateral bending compared with experimental data from Panjabi *et al.* [37]. (d) The updated upper cervical spine C0–C2 complex in flexion–extension in comparison with data from [38], and in axial rotation (e) and lateral bending (f) compared with data from [37].

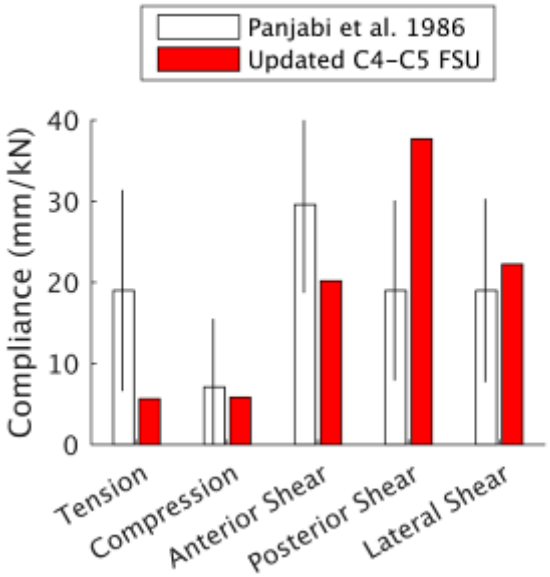

Fig. C3. Compliance of the updated C4–C5 FSU evaluated as the ratio of the displacement for an applied load of 25 N and compared with experimental data from Panjabi *et al.* [39].

The response of the assembled ligamentous cervical spine from C0 to the first thoracic vertebra T1 was partially assessed with respect to experimental data. Yoganandan *et al.* [40] tested four human C0–T3 human cervical spines, with an average stiffness of 0.059 kN/mm, to failure in tension. The updated C0–T1 model was of the same order of magnitude in stiffness (0.119 kN/mm) as the stiffest of these subjects (Fig. C4). Hence, it seems to compare reasonably well as the two thoracic vertebra segments would add some additional compliance to the simulation result.

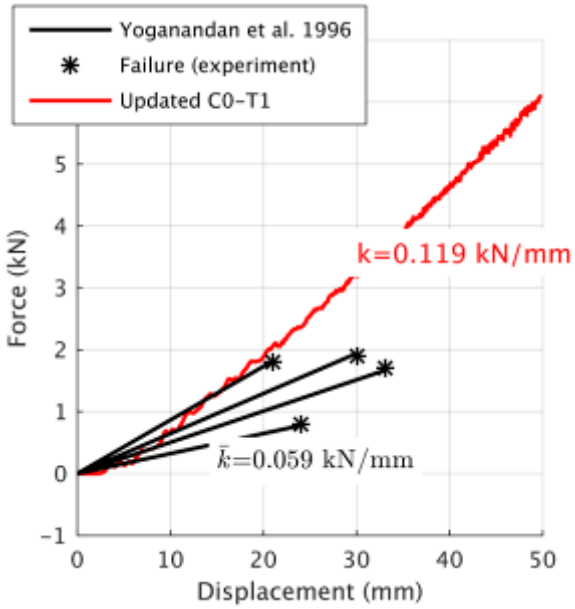

Fig. C4. Tensile response of the C0–T1 ligamentous spine compared with linear extrapolation of test data reported for human ligamentous C0–T3 specimens by Yoganandan *et al*. [40].

Appendix C References

[32]Yoganandan N, Pintar FA, Stemper BD, Baisden JL, Aktay R, Shender BS, Paskoff G, Laud P. (2006) Trabecular Bone Density of Male Human Cervical and Lumbar Vertebrae. *Bone*, **39**(2):336–344.

[33]Yoganandan N, Kumarsean S, Pintar FA. (2000) Geometric and Mechanical Properties of the Human Cervical Spine Ligaments. *Journal of Biomechanical Engineering*, **122**:623–629.

[34]Mattucci SFE, Cronin DS. (2015) A Method to Characterize Average Cervical Spine Ligament Response Based on Raw Data Sets for Implemenation Into Injury Biomechanics Models. *Journal of the Mechanical Behavior of Biomedical Materials*, **41**:216–226.

[35]Mattucci SFE, Moulton JA, Chandrashekar N, Cronin DS. (2013) Strain Rate Dependent Properties of Human Craniovertebral Ligaments. *Journal of the Mechanical Behavior of Biomedical Materials*, **23**: 71–79.

[36]Myklebust JB, Pintar F, Yoganandan N, Cusick JF, Maiman D, Myers TJ, Sances A. (1988) Tensile Strength of Spinal Ligaments. *Spine*, **13**(5):525–531.

[37]Panjabi MM, Crisco JJ, Vasavada A, Oda T, Cholewicki J, Nibu K, Shin E. (2001) Mechanical Properties of the Human Cervical Spine as Shown by Three-Dimensional Load-Displacement Curves. *Spine,* **26**(24):2692–2700.

[38]Nightingale RW, Chancey VC, Ottaviano D, Luck JF, Tran L, Prange M, Myers BS. (2007) Flexion and Extension structural properties and strengths for male cervical spine segments. *Journal of Biomechanics,* **40**:535–542.

[39]Panjabi MM, Summers DJ, Pelker RR, Videman T, Friedlaender GE, Southwick WO. (1986) Three-Dimensional Load–Displacement Curves Due to Forces on the Cervical Spine. *Journal of Orthopaedic Research*, **4**:152–161.

[40]Yoganandan N, Pintar FA, Maiman DJ, Cusick JF, Sances A, Walsh PR. (1996) Human Head-Neck Biomechanics under Axial Tension. *Medical Engineering Physics*, **18**(4): 289–294.

XI. APPENDIX D – MUSCLE ACTIVATIONS AND FORCES

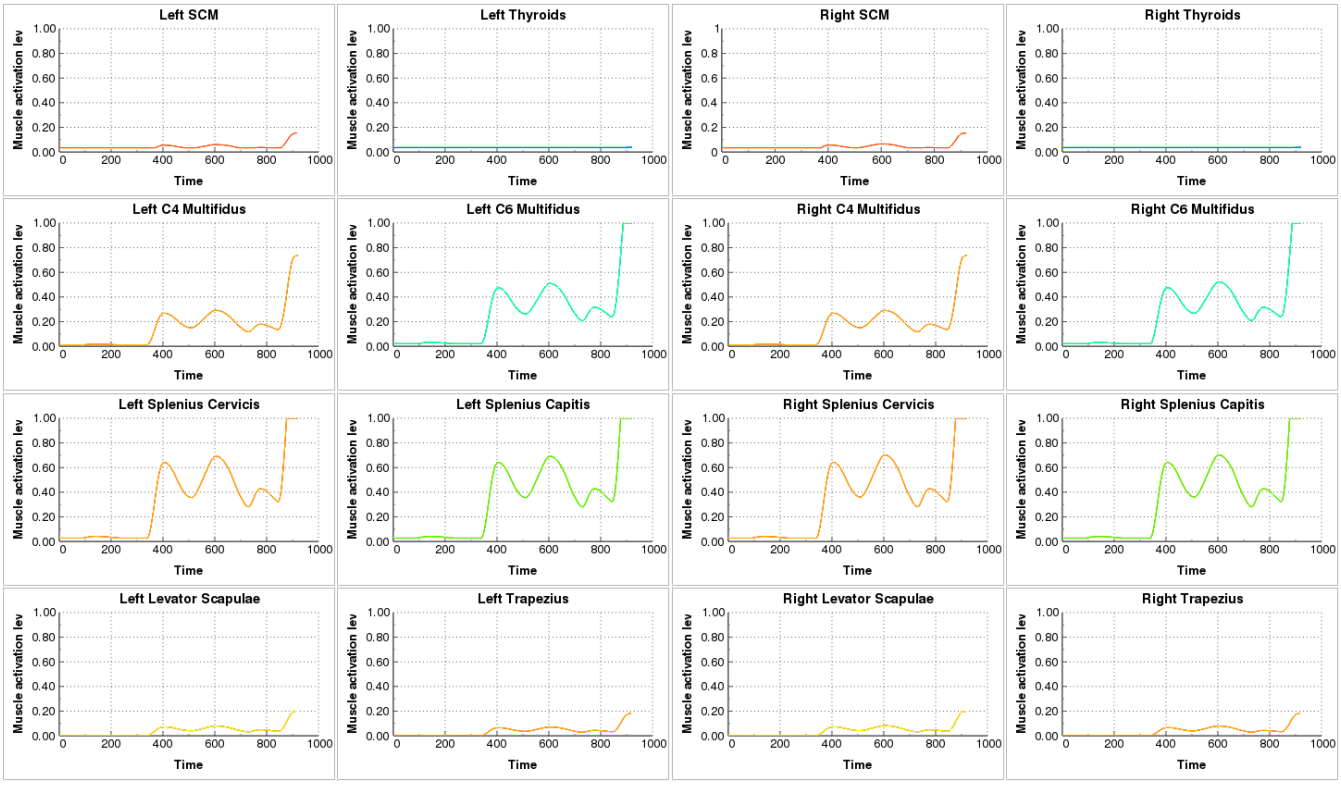

Fig. D1. Cervical muscle activations during Simulation 9 (repositioning at 80°/s prior to crash). The first 300 ms represent the settling simulation time for the active HBM, and the last 120 ms the crash phase.

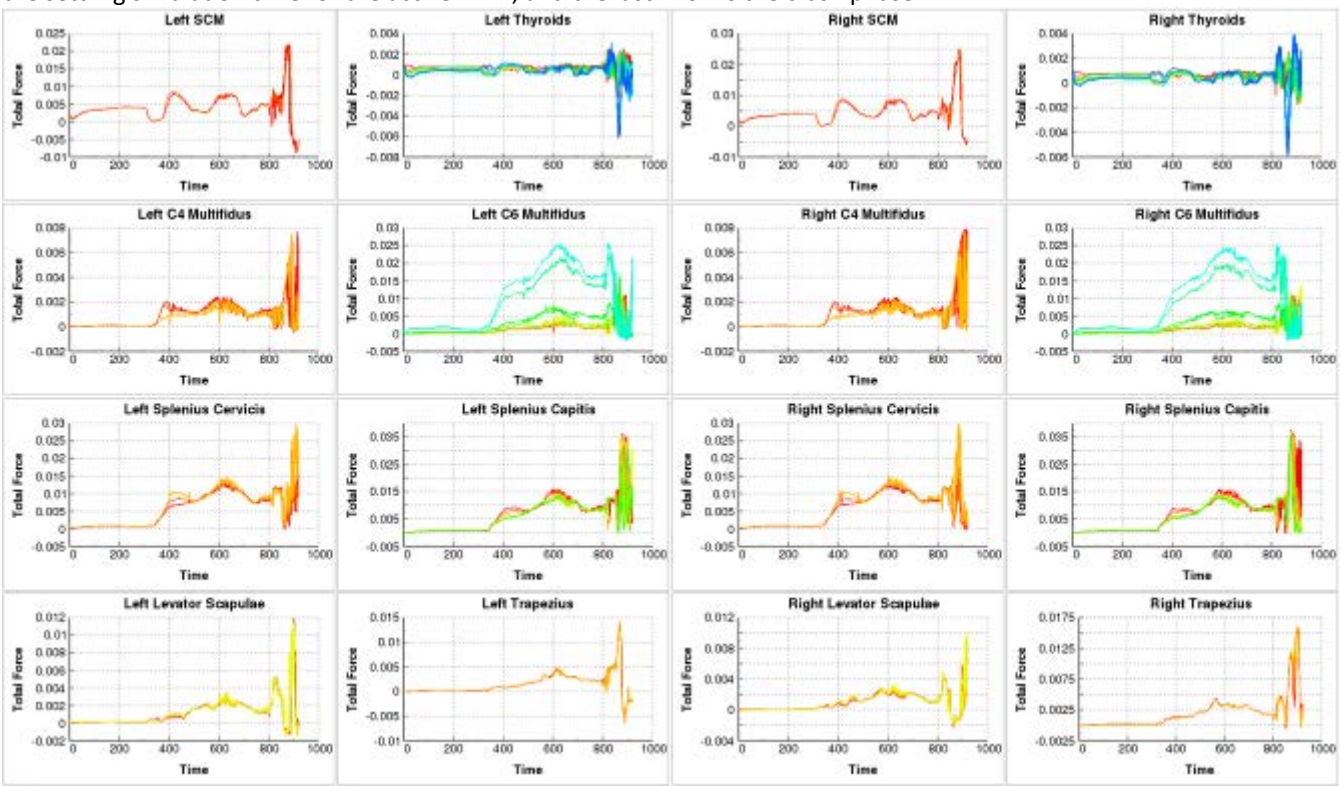

Fig. D2. Cervical muscle forces during Simulation 9 (repositioning at 80°/s prior to crash). The first 300 ms represent the settling simulation time for the active HBM, and the last 120 ms the crash phase.

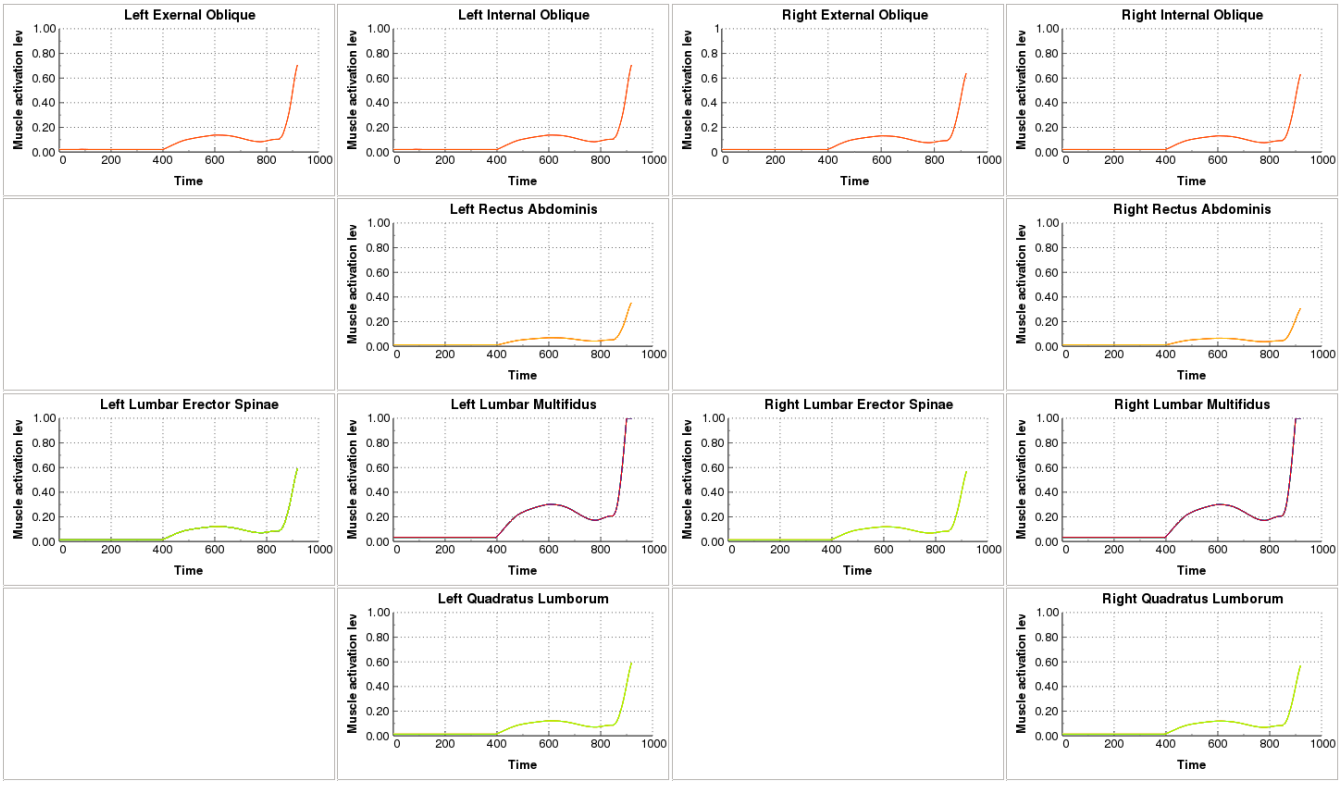

Fig. D3. Lumbar and abdominal muscle activations during Simulation 9 (repositioning at 80°/s prior to crash). The first 300 ms represent the settling simulation time for the active HBM, and the last 120 ms the crash phase.

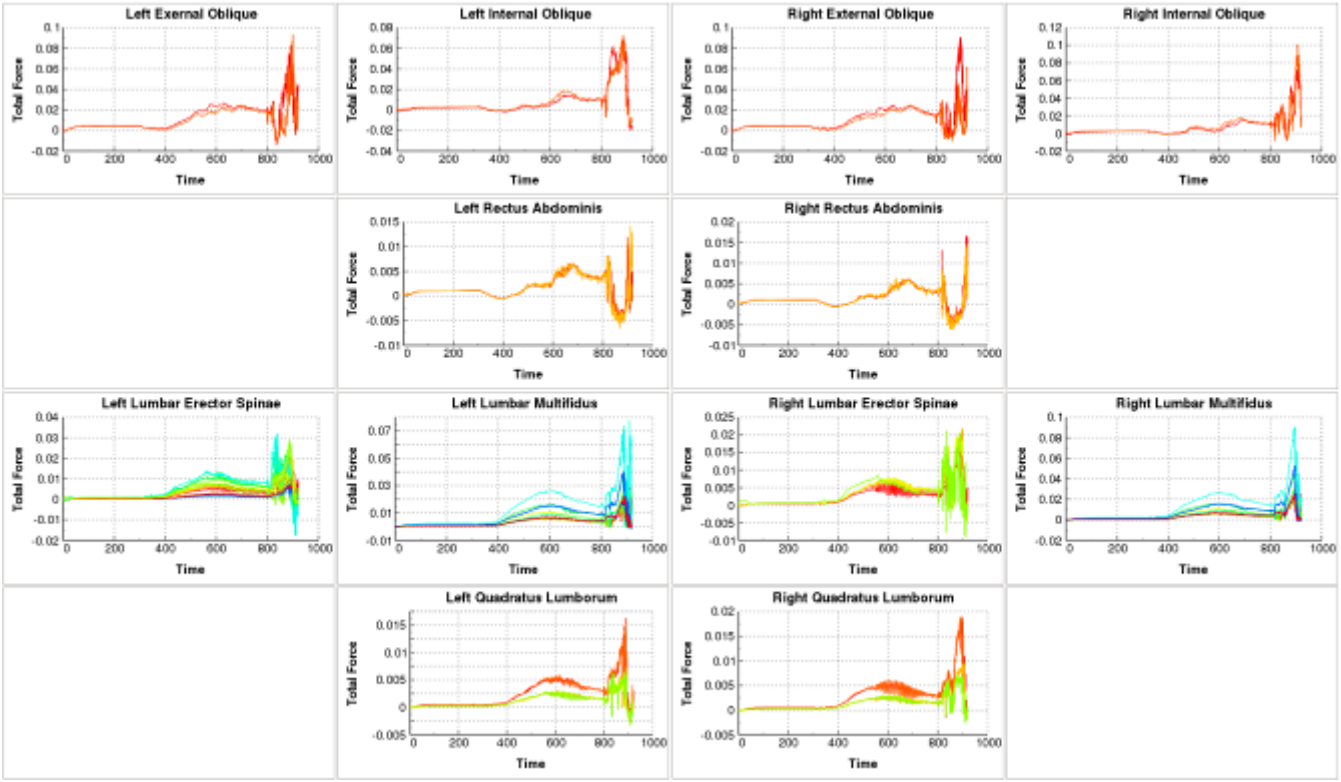

Fig. D4. Lumbar and abdominal muscle forces during Simulation 9 (repositioning at 80°/s prior to crash). The first 300 ms represent the settling simulation time for the active HBM, and the last 120 ms the crash phase.

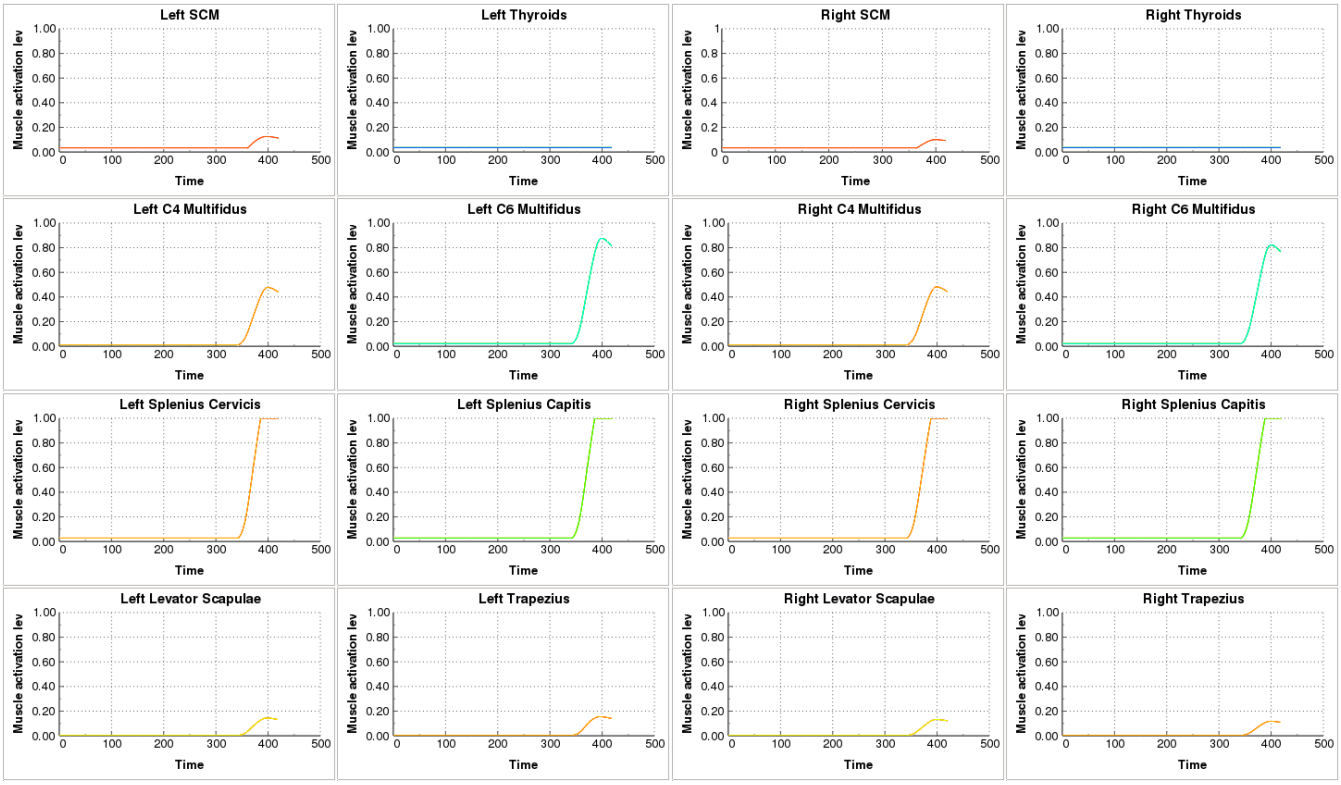

Fig. D5. Cervical muscle activations during Simulation 3 (upright without any pre-crash maneuver). The first 300 ms represent the settling simulation time for the active HBM, and the last 120 ms the crash phase.

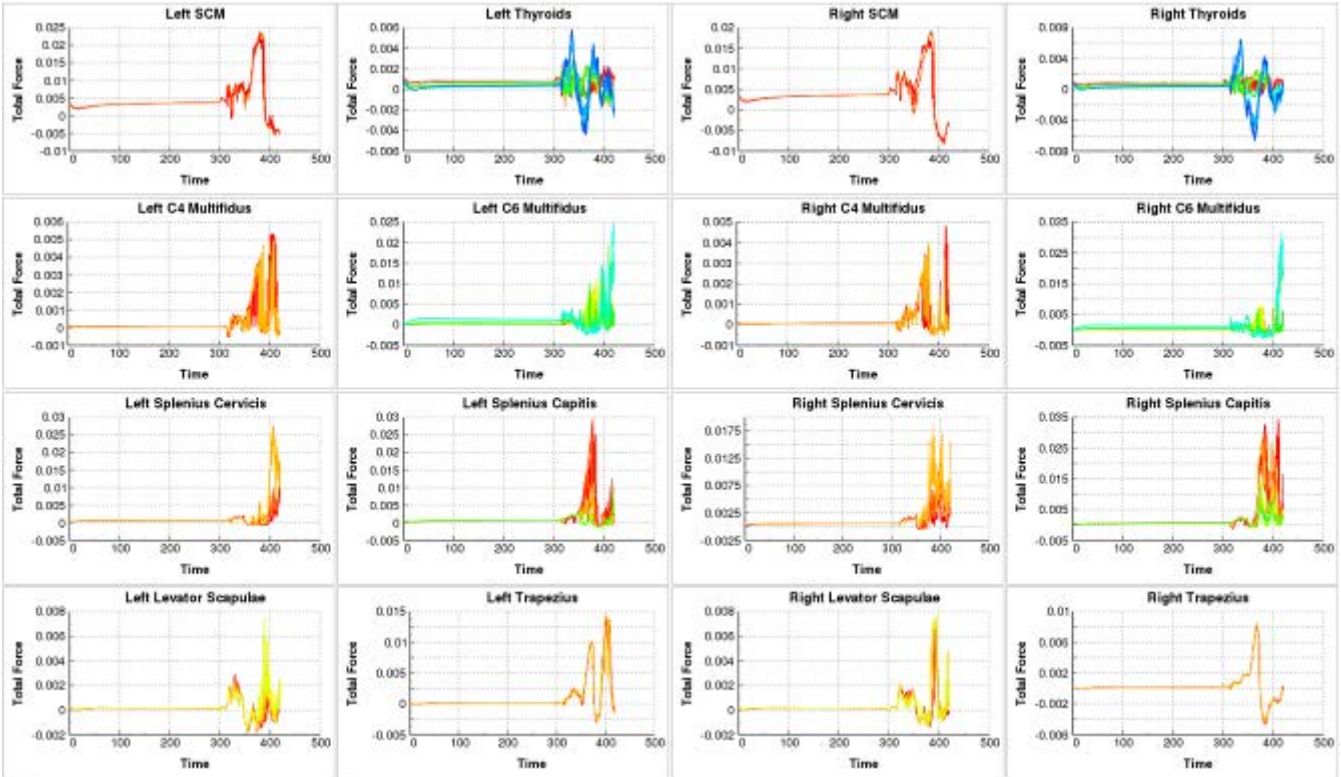

Fig. D6. Cervical muscle forces for all muscle elements during Simulation 3 (upright without any pre-crash maneuver). The first 300 ms represent the settling simulation time for the active HBM, and the last 120 ms the crash phase.

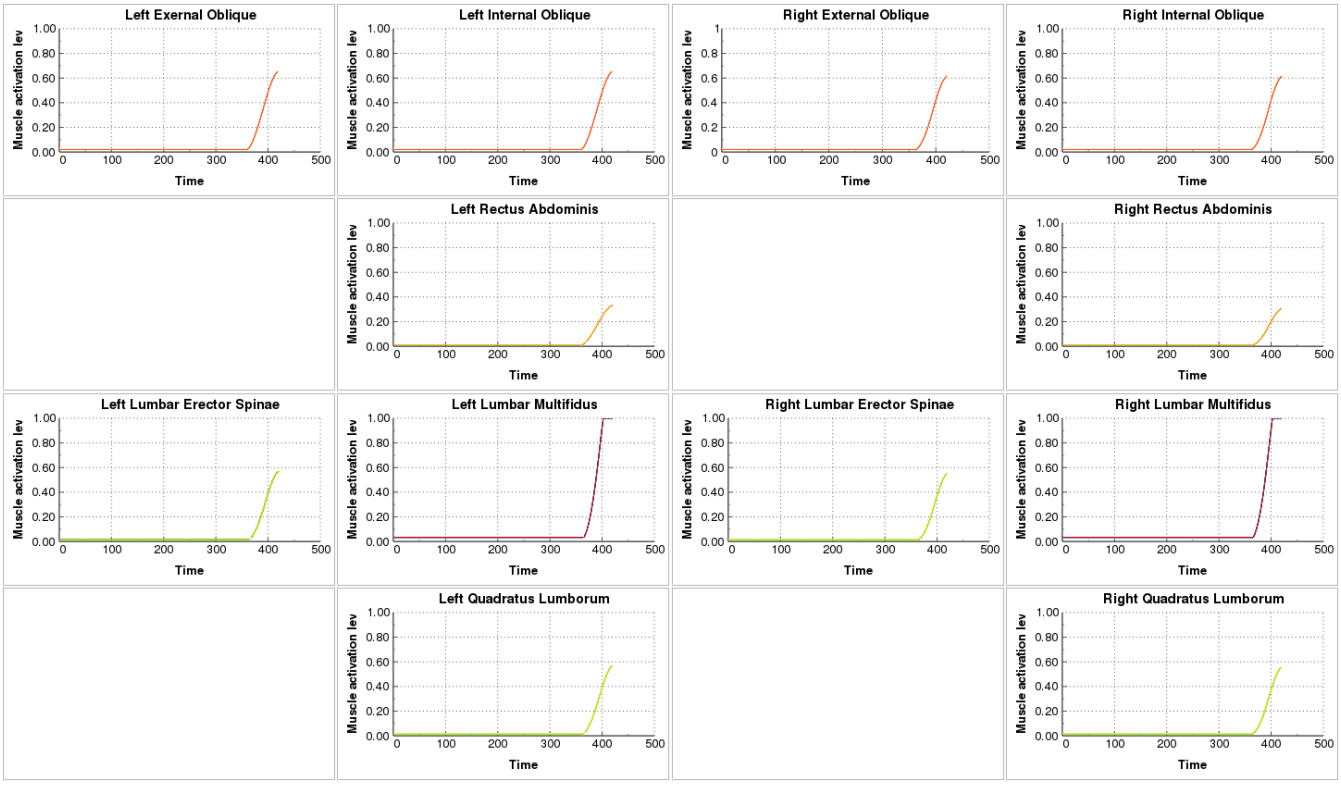

Fig. D7. Lumbar and abdominal muscle activations during Simulation 3 (upright without any pre-crash maneuver). The first 300 ms represent the settling simulation time for the active HBM, and the last 120 ms the crash phase.

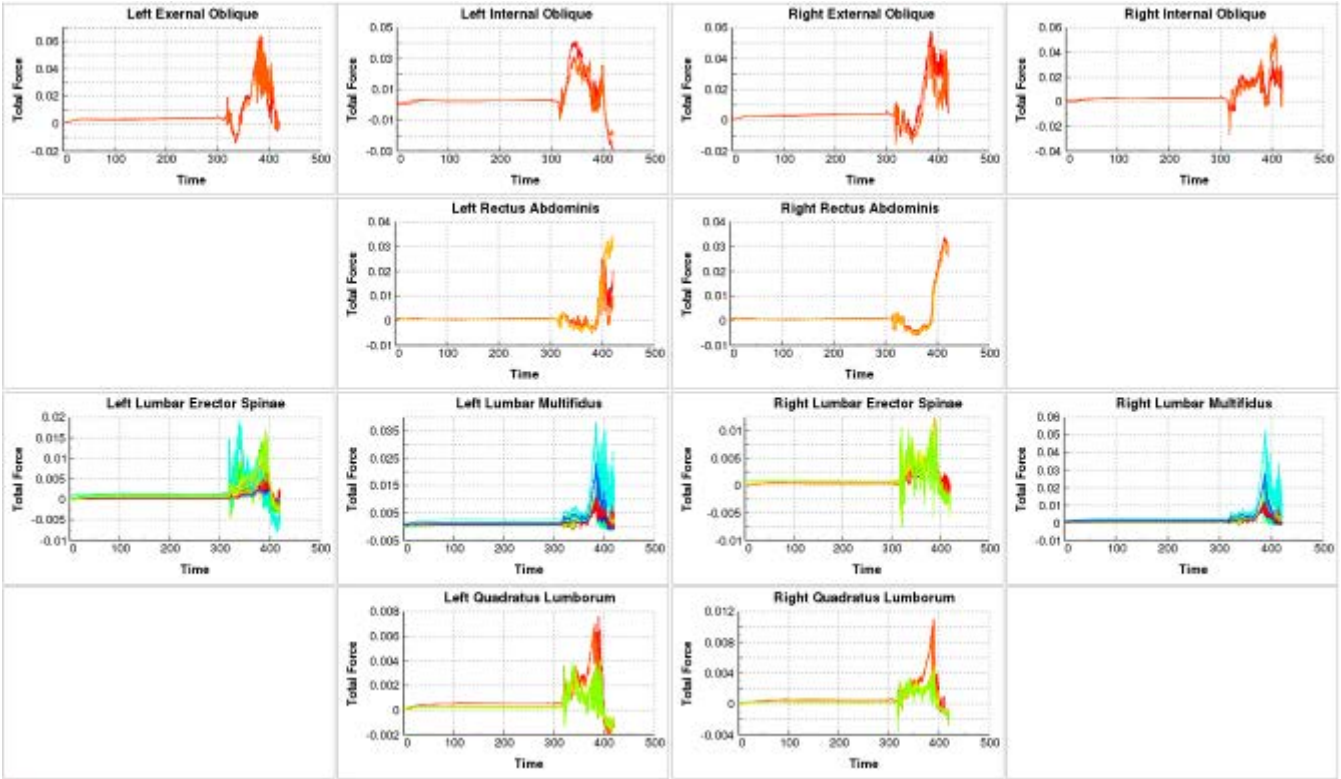

Fig. D8. Lumbar and abdominal muscle forces for all muscle elements during Simulation 3 (upright without any pre-crash maneuver). The first 300 ms represent the settling simulation time for the active HBM, and the last 120 ms the crash phase.